NASA/TM—2011-216832 AIAA–2010–4823

Assessment of Computational Fluid Dynamics (CFD) Models for Shock Boundary-Layer Interaction

James R. DeBonis
Glenn Research Center, Cleveland, Ohio

William L. Oberkampf
WLO Consulting, Austin, Texas

Richard T. Wolf, Paul D. Orkwis, and Mark G. Turner
University of Cincinnati, Cincinnati, Ohio

Holger Babinsky
University of Cambridge, Cambridge, United Kingdom

March 2011

NASA STI Program . . . in Profile

Since its founding, NASA has been dedicated to the advancement of aeronautics and space science. The NASA Scientific and Technical Information (STI) program plays a key part in helping NASA maintain this important role.

The NASA STI Program operates under the auspices of the Agency Chief Information Officer. It collects, organizes, provides for archiving, and disseminates NASA's STI. The NASA STI program provides access to the NASA Aeronautics and Space Database and its public interface, the NASA Technical Reports Server, thus providing one of the largest collections of aeronautical and space science STI in the world. Results are published in both non-NASA channels and by NASA in the NASA STI Report Series, which includes the following report types:

- TECHNICAL PUBLICATION. Reports of completed research or a major significant phase of research that present the results of NASA programs and include extensive data or theoretical analysis. Includes compilations of significant scientific and technical data and information deemed to be of continuing reference value. NASA counterpart of peer-reviewed formal professional papers but has less stringent limitations on manuscript length and extent of graphic presentations.

- TECHNICAL MEMORANDUM. Scientific and technical findings that are preliminary or of specialized interest, e.g., quick release reports, working papers, and bibliographies that contain minimal annotation. Does not contain extensive analysis.

- CONTRACTOR REPORT. Scientific and technical findings by NASA-sponsored contractors and grantees.

- CONFERENCE PUBLICATION. Collected papers from scientific and technical conferences, symposia, seminars, or other meetings sponsored or cosponsored by NASA.

- SPECIAL PUBLICATION. Scientific, technical, or historical information from NASA programs, projects, and missions, often concerned with subjects having substantial public interest.

- TECHNICAL TRANSLATION. English-language translations of foreign scientific and technical material pertinent to NASA's mission.

Specialized services also include creating custom thesauri, building customized databases, organizing and publishing research results.

For more information about the NASA STI program, see the following:

- Access the NASA STI program home page at *http://www.sti.nasa.gov*

- E-mail your question via the Internet to *help@sti.nasa.gov*

- Fax your question to the NASA STI Help Desk at 443–757–5803

- Telephone the NASA STI Help Desk at 443–757–5802

- Write to:
  NASA Center for AeroSpace Information (CASI)
  7115 Standard Drive
  Hanover, MD 21076–1320

NASA/TM—2011-216832 AIAA–2010–4823

Assessment of Computational Fluid Dynamics (CFD) Models for Shock Boundary-Layer Interaction

James R. DeBonis
Glenn Research Center, Cleveland, Ohio

William L. Oberkampf
WLO Consulting, Austin, Texas

Richard T. Wolf, Paul D. Orkwis, and Mark G. Turner
University of Cincinnati, Cincinnati, Ohio

Holger Babinsky
University of Cambridge, Cambridge, United Kingdom

Prepared for the
28th Applied Aerodynamics Conference
sponsored by the American Institute of Aeronautics and Astronautics
Chicago, Illinois, June 28 to July 1, 2010

National Aeronautics and
Space Administration

Glenn Research Center
Cleveland, Ohio 44135

March 2011

Acknowledgments

The authors would like to thank all of those who contributed solutions their solutions for this study. The significant time and effort that is represented by each solution is greatly appreciated. The authors would also like to thank the experimentalists who provided their data for the effort. In particular, Ethan Eagle and Evan Bonny provided valuable insight that assisted in the uncertainty analysis of their experiments at the University of Michigan.

This report is a formal draft or working paper, intended to solicit comments and ideas from a technical peer group.

This report contains preliminary findings, subject to revision as analysis proceeds.

Level of Review: This material has been technically reviewed by technical management.

Available from

NASA Center for Aerospace Information
7115 Standard Drive
Hanover, MD 21076–1320

National Technical Information Service
5301 Shawnee Road
Alexandria, VA 22312

Available electronically at http://www.sti.nasa.gov

Assessment of Computational Fluid Dynamics (CFD) Models for Shock Boundary-Layer Interaction

James R. DeBonis
National Aeronautics and Space Administration
Glenn Research Center
Cleveland, Ohio 44135

William L. Oberkampf
WLO Consulting
Austin, Texas 78633

Richard T. Wolf, Paul D. Orkwis, and Mark G. Turner
University of Cincinnati
Cincinnati, Ohio 45221

Holger Babinsky
University of Cambridge
Cambridge, United Kingdom, CB2 1PZ

Abstract

A workshop on the computational fluid dynamics (CFD) prediction of shock boundary-layer interactions (SBLIs) was held at the 48th AIAA Aerospace Sciences Meeting. As part of the workshop numerous CFD analysts submitted solutions to four experimentally measured SBLIs. This paper describes the assessment of the CFD predictions. The assessment includes an uncertainty analysis of the experimental data, the definition of an error metric and the application of that metric to the CFD solutions. The CFD solutions provided very similar levels of error and in general it was difficult to discern clear trends in the data. For the Reynolds Averaged Navier-Stokes methods the choice of turbulence model appeared to be the largest factor in solution accuracy. Large-eddy simulation methods produced error levels similar to RANS methods but provided superior predictions of normal stresses.

Nomenclature

u, v, w	streamwise, transverse and spanwise velocity components
x, y, z	cartesian coordinates
$E(f)$	error metric of f
M_∞	freestream Mach number
p_0	stagnation pressure
T_0	stagnation temperature
Re_θ	Reynolds number based on momentum thickness
U_∞	freestream velocity
$< u'^2 >$	streamwise normal stress
$< v'^2 >$	transverse normal stress
$< u'v' >$	shear stress
δ	boundary-layer thickness
θ	shock deflection angle
Δx, Δy, Δz	spacing of PIV measurement grid

subscripts

cfd	computational fluid dynamics obtained quantity
exp	experimentally obtained quantity

I. Introduction

A shock boundary-layer interaction (SBLI) is an important and complex fluid dynamic phenomena that occurs in supersonic flows. It is one of the primary flow features in supersonic inlets, and if not controlled, can have a major impact on inlet performace. Predicting SBLIs and understanding how to control them is a critical technology area for development of propulsion systems for supersonic vehicles. The United States Air Force, the National Aeronautics and Space Administration (NASA) and numerous aerospace companies are developing and researching supersonic vehicles.

The SBLI considered in this study consists of an oblique shock wave, impinging on a supersonic flow over a wall which has formed a turbulent boundary layer. The shock wave imposes an abrupt adverse pressure gradient. This pressure gradient negatively affects the boundary layer, thickening the layer and perhaps separating the boundary layer from the wall. The interaction increases turbulence levels in the boundary layer and typically induces unsteadiness in the shock wave. In wind tunnels and inlets with rectangular cross-sections the shock also affects the sidewall boundary layer and corner flows resulting in extremely complex three-dimensional flowfields. An excellent description of the phenomena is given by Delery and Marvin.[1] In a supersonic inlet the SBLI creates total pressure loss, flow distortion and in the case of mixed- and internal-compression inlets the increased potential of inlet unstart (reduced stability).

The phenomena is complex and difficult to predict using computational fluid dynamics (CFD). Traditionally Reynolds Averaged Navier-Stokes (RANS) CFD methods have been used for SBLI predictions. RANS methods rely on models to simulate the effect of the turbulence on the mean flow. These models are developed and adapted for well-behaved boundary layers and shear layers and can not accurately model the complex flow in a SBLI. Large-eddy simulation (LES), a technique which directly computes the large-scale turbulence, offers the promise for improved predictions but is just now becoming a practical option for these types of flows due to increased computing power.

A workshop on the CFD prediction of shock boundary-layer interactions was organized by the American Institute of Aeronautics and Astronautics (AIAA).[2–4] The workshop was held at the 48th AIAA Aerospace Sciences Meeting in Orlando, Florida. The purpose of the workshop was to share prediction methodologies, assess the state of the art in SBLI prediction and determine the most promising methods. Four test cases with extensive experimental data were identified and the geometry and flow conditions for each were provided to the analysts. The experimental data was also provided for two cases - the cases with the weakest shock interactions. The data was held back for the two cases with the strongest shock interaction, to assess the solutions in a true predictive situation. A key component of this effort was to provide an objective assessment of the error for each of the predictions. This paper discusses the assessment of the CFD predictions for the four SBLI workshop cases. The assessment includes an evaluation of the experimental uncertainty, a definition of an error metric, the results of the error assessment for each test case and a discussion of some trends that were identified in the data.

II. Experimental Data

The data used in the workshop came from two sources. The general setup of the experiment was similar for both (Fig. 1). A shock generator plate was placed in the test section of a supersonic wind tunnel at an angle to the freestream flow. This angle, θ, is the shock deflection angle, which determines the strength of the oblique shock wave. A turbulent boundary layer is present on the floor of the wind tunnel. An oblique shock wave is formed by the plate and intersects the boundary layer. Particle Image Velocimetry (PIV) measurements of velocities and turbulent quantities were performed in the region of the shock boundary-layer interaction. The use of PIV, a relatively new technique, for comparison to CFD represents an advance in the assessment of CFD for SBLIs. Typically wall pressure and skin friction data has been used. PIV provides a much more detailed look at the flow. Table 1 summarizes the experimental cases.

The geometries for both test setups were provided in IGES format. The basic layouts of the tunnels and shock generator plates, based on the IGES files, are shown in Fig. 2. A comparison of the wind tunnel cross-sections including the shock generator plate and boundary-thickness are given in Fig. 3.

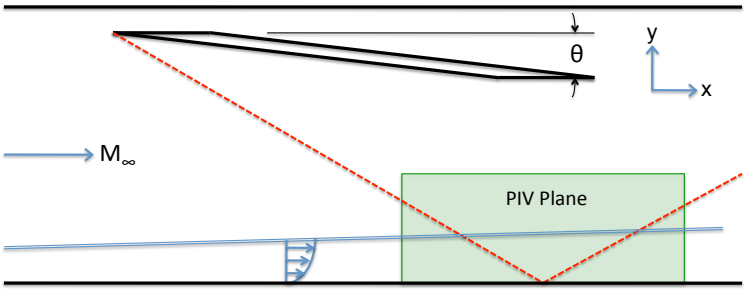

Figure 1. Schematic of a SBLI in a supersonic wind tunnel

Organization	M_∞	θ (deg.)	T_0 (K)	p_0 (kPa)	Re_θ	
IUSTI Marseille (UFAST)	2.25	8.0	293	50.5	6,900	open
University of Michigan (CCAS)	2.75	7.75	293	101	6,600	open
University of Michigan (CCAS)	2.75	10.0	293	101	6,600	blind
University of Michigan (CCAS)	2.75	12.0	293	101	6,600	blind

Table 1. Summary of the experimental cases

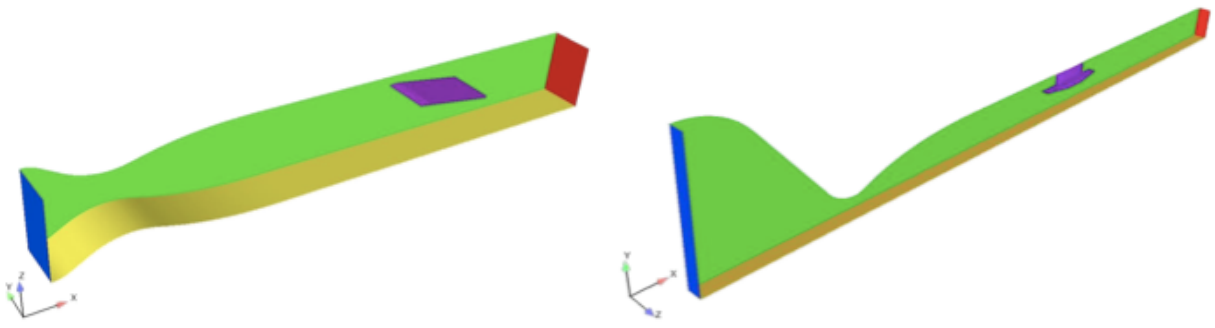

(a) IUSTI (b) UMich

Figure 2. Wind tunnel and shock generator layout (courtesy of Vishal Bhagwandin, Army Research Laboratory)

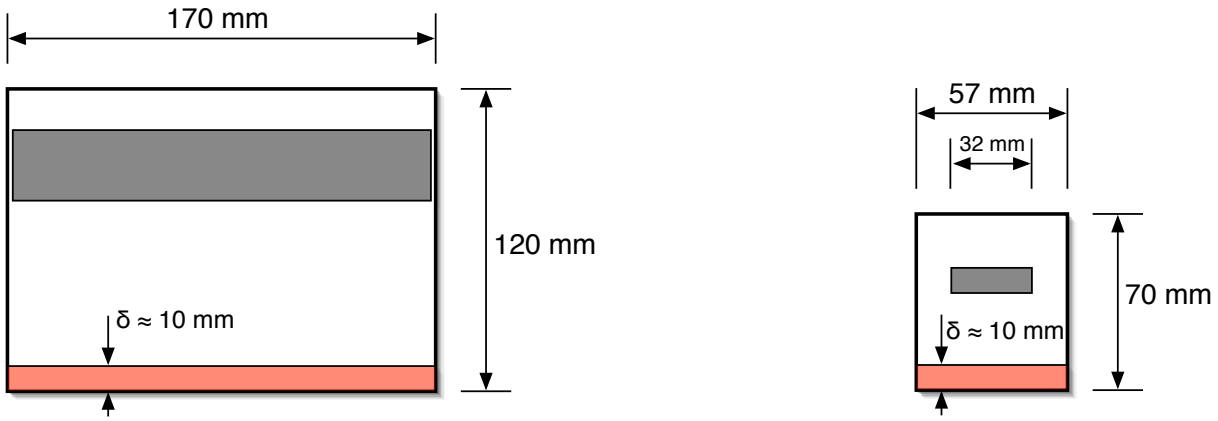

(a) IUSTI (b) UMich

Figure 3. Comparison of wind tunnel cross-sections

The two experimental datasets are summarized below. Details of the PIV measurements and their effect on the experimental uncertainty are given in the following section (Sec. III).

A. IUSTI Mach 2.25 – 8.0 degree case

The first dataset was taken at the Institut Universitaire des Systèmes Thermiques Industriels (IUSTI) in Marseille, France.[5] This data was also used as the test case for the European Union sponsored research effort on SBLIs named UFAST.[6] The freestream Mach number, M_∞, was 2.25 and the deflection angle was 8.0 degrees. The wind tunnel nozzle has converging/diverging walls on both the upper and lower surfaces and straight sidewalls (Fig. 2(a)). The wind tunnel test section was 120 mm high and 170 mm wide. The shock generator plate spanned the width of the tunnel, with only a small gap between the plate and tunnel sidewalls. The data taken included 2D PIV, stereoscopic PIV, laser doppler velocimetry (LDV) and wall pressures. The data used here for comparison is the PIV data on a streamwise plane (a plane parallel to the freestream flow and the tunnel sidewall) in the center of the tunnel. The PIV plane was limited to only the interaction region. The LDV measurements were used to verify the PIV data. The data provided for comparison included: streamwise and transverse velocities, u and v, normal stresses, $\sqrt{< u'^2 >}$ and $\sqrt{< v'^2 >}$ and shear stress, $- < u'v' >$.

B. UMich. Mach 2.75 – 7.75, 10.0 and 12.0 degree cases

The remaining datasets were taken at the University of Michigan (UMich.)[7] The UMich effort is part of the U.S. Air Force sponsored Collaborative Center for the Aeronautical Sciences (CCAS). The freestream Mach number, M_∞, was 2.75. The shock generator plate was set at three different angles, 7.75, 10.0 and 12.0 degrees, increasing the strength of the shock and the size of the interaction. The upper wall of the wind tunnel served as the converging diverging nozzle (Fig. 2(b)). The wind tunnel test section was 70 mm high and 57 mm wide. The shock generator plate was 32 mm wide and spanned the center portion of the tunnel (Fig. 3(b)). The narrower plate is an attempt to avoid strong shock boundary-layer interactions on the tunnel sidewalls. The test section is narrower than the IUSTI test section and the boundary layer and shock generator create a larger percentage of blockage for the tunnel flow. One would expect significant influence of the corner flows on the tunnel centerline and a more three-dimensional flowfield. The data consists of stereo PIV measurements on a streamwise plane in the center of the tunnel and several spanwise planes (Fig. 4). The PIV planes include the interaction region and a portion of the freestream flow above. In addition, a streamwise data plane was provided to characterize the boundary layer upstream of the interaction. The data provided included: streamwise, transverse and spanwise velocities, u, v and w, normal stresses, $< u'^2 >$, $< v'^2 >$ and $< w'^2 >$, shear stresses, $< u'v' >$, $< u'w' >$, and $< v'w' >$ and velocity gradients. Note that there is a difference between the two experiments in the form of the turbulent stresses.

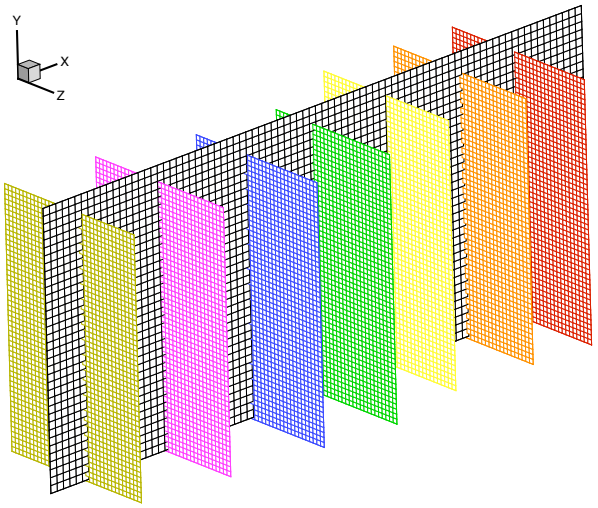

Figure 4. Streamwise and spanwise planes for PIV measurements for the UMich. data

III. Experimental Uncertainty Estimation

This section discusses how the uncertainties in the experimental measurements from IUSTI and UMich. were estimated. For the IUSTI experiment, an estimate of the experimental uncertainty was obtained from Dussage et al.[8] and for the and for the UMich. experiment, an estimate of uncertainty was obtained from Lapsa and Dahm.[7] We also applied an independent method to estimate experimental uncertainty developed by Oberkampf and coworkers[9–11] to the UMich. Data. The method is based entirely on statistically analyzing the differences in multiple measurements of the various quantities of interest, e.g., u, v, w, as well as normal stresses and shear stresses.

A. IUSTI Data Uncertainty

Spatial resolution of the stereoscopic PIV technique is limited by the thickness of the laser lightsheet (1 mm) and the size of the analysis windows. The final effective cell size is 16 (horizontal) x 8 (vertical) pixels, leading to the data being averaged over a volume of 1 mm x 0.5 mm, and a light sheet thickness of 1 mm. No detailed analysis of the uncertainty in the velocity measurements was provided, but the estimated uncertainty is quoted as 6 m/s.[5] This value of uncertainty was used in the comparisons of CFD results with IUSTI measurements.

An independent assessment of the accuracy of the PIV measurements was obtained by a number of comparisons with LDV measurements for the same conditions in the wind tunnel. It was found that with the initial field of view for the PIV that large errors occurred in measured velocities. After the field of view was significantly reduced, they found good agreement between PIV and LDV measurements for both mean velocities as well as turbulent stresses.

B. UMich. Data Uncertainty

The parameters for the PIV set-up at the University of Michigan were similar to those used in the IUSTI experiments, except that data were obtained by stereoscopic PIV along a streamwise plane as well as seven spanwise planes. The streamwise field of view covers a significantly larger region than each spanwise slice and for this reason the PIV window size and operating parameters differ. In the streamwise plane a window of 32x32 pixels (the smallest used in the analysis) was approximately equivalent to 1 mm x 1 mm window size and the light sheet thickness was 0.5mm. A delay of about 1 μs was set between the two laser pulses. Spanwise planes use a smaller field of view to obtain better spatial resolution and as a result window sizes were 0.5 mm x 0.5 mm and the time increment between two laser pulses was around 500 ns.

No comprehensive uncertainty analysis was provided for the measurements, nor were the PIV measurements compared with an independent technique. However, the repeatability of the measurements was assessed by comparing the results of different test campaigns performed several weeks apart. The different test campaigns involved completely independent forming and positioning of the laser sheets, positioning of the stereo cameras, calibration of the camera fields-of-view, and all other aspects associated with set-up and calibration of the experiment. Comparison of the two results through the boundary layer showed that the mean u component of velocity was indiscernible between the two campaigns, except for the first three points near the wall. Comparisons for the mean v component of velocity showed a maximum difference of 9 m/s and the average difference through the boundary layer of 3 m/s.

One particular issue of concern emerged in recent months due to the work of Ethan Eagle and Evan Bonny of the Dept. of Aerospace Engineering, University of Michigan, working with the same stero-PIV instrumentation. The spanwise high-resolution measurements in particular required very short time intervals between the two laser pulses (500 nm) which are at the limit of what is possible with today's technology. This was recognized by the original researchers who measured the actual time delay between two laser pulses at the start of the investigation and reported that this was somewhat larger than commanded by the software. However, subsequent research by Eagle and Bonny found that the hardware used for the experiments was less reliable than previously thought and that the actual delay fluctuates more significantly, giving a velocity bias error that is directly proportional to the timing discrepancy. It was found that there is on average an additional time delay of up to 50 ns and a shot-to-shot variation of the order of 10-15 ns. The original data was obtained with only a single measurement of this timing delay and it is therefore likely that it suffers from both a systematic bias error and a random fluctuating error. For the data taken along the spanwise planes these errors might be as large as 10-13%, while the streamwise plane data (which was taken with larger interval times) may be affected by about half of these estimates. For this reason only the streamwise planes are used for comparison in this paper. This topic will be revisited in the next section.

C. Statistical Estimation Method

A completely different approach for estimating the experimental uncertainty of measurements obtained in wind tunnels has been developed by Oberkampf and coworkers.[9–11] This technique is a statistical approach that is based on analyzing comparisons of multiple measurements of quantities of interest. It is usually referred to as statistical design of experiments (DOE) because it analyzes the final measured result of the quantities of interest, based on specially designed sampling techniques.[12,13] We were able to apply this technique to the published UMich. data and take advantage of the fact that the sampling is derived from two different planes. Here we will only give a brief description of the approach, the key computational steps, and the results of the analysis.

The approach compares measurements of each of the quantities of interest that are obtained from both the streamwise and spanwise planes. The quantities of interest can be either directly measured quantities, i.e., mean velocity components u, v, w, and u', v', w', or they can be quantities derived from the measurements, such as gradients of these quantities or Reynolds stresses. At each of the seven intersections of the spanwise planes with the streamwise plane, and for each of the three shock generator angles, the uncertainty in the quantities of interest can be estimated.

This statistical approach could also be applied to comparisons between multiple measurements of the same quantity in the same plane. This calculation would independently estimate the repeatability uncertainty that was discussed above (Sec. B). It is well known that this type of repeatability uncertainty, also referred to as 0th order replication,[14] is smaller, sometimes much smaller, than the total uncertainty due to other sources in an experiment. Although this calculation was not done for the UMich. experiment, it is planned for future work because the repeatability data has been archived.

When comparisons are made between multiple measurements of the same quantity in different planes, then in addition to the repeatability uncertainty just mentioned, one can capture a wider range of systematic (bias) uncertainties. Examples of these systematic uncertainties are any changes in the calibration procedure of the PIV system (such as spatial positioning of the laser sheet or measurement volume), changes in the optical setup of the laser sheet used in the PIV system, and changes in PIV window size or spatial resolution. The effect of these types of systematic uncertainties on the quantities of interest can be quantified by using streamwise and spanwise measurements because now we have sampled correlated bias uncertainties that arise from different populations. That is, anytime in an experiment that the quantities of interest can be measured where some source of uncertainty can be altered, then we are sampling from a modified population.

The more independent each modified population is, the more accurate we are in estimating the true (total) uncertainty. For example, more independence of the sources of correlated bias uncertainties can be obtained if one were to measure the velocity components with an LDV technique, or make measurements using a hot wire technique in a separate wind tunnel facility.

To make comparisons of quantities of interest at the intersection of two planes, one must interpolate both planes of data to common points in space so that a proper assessment of uncertainty is made. We used bi-linear interpolation in each plane of data to obtain each quantity of interest at the following intersection points; x is defined by the x value of the spanwise plane of data, y is defined by the y value of the streamwise plane of points, and z is defined by $z = 0$ (the z coordinate the streamwise plane. The spacing of the measurement points in the streamwise plane was $\Delta x = \Delta y = 0.5024$ mm and in the spanwise plane it was $\Delta y = \Delta z = 0.2879$ mm. As a result, the bi-linear interpolation of the measurements required no more than half of each of these distances for the interpolation.

Figure 5 shows the residuals of the u, v, and w mean velocity components for the 21 streamwise and spanwise plane intersections (seven spanwise plane intersections for each of the three shock generator angles). Since each intersection has 30 - 35 measurement points in the streamwise plane, this yields a total 681 residuals for each quantity of interest. The residual in Fig. 5 is the difference between the measurement of the quantity in each plane, and the abscissa is the average value of the measured quantity in both planes. None of the scatter plots show any clear trend with regard to how the residual changes as a function of magnitude of velocity, or how it varies with the deflection angle. The v and w plots show a slight trend of decreasing residuals as a function of magnitude of velocity. It is believed that the random and bias error in the shot-to-shot timing of the two laser pulses mentioned above is responsible for the large scatter in the residuals, particularly for the low magnitudes of velocity.

Also shown in each figure is the mean and standard deviation of the nondimensional residuals. As can be seen, the mean of the u residuals is about four times larger than the mean of v and w. The nondimensional mean uncertainty for v and w are seen to be very similar. Converting these means to dimensional quantities, the u, v, and w uncertainty means are 20.94 m/s, 5.40 m/s, and 3.67 m/s, respectively. As expected, the statistical uncertainty in u is larger than the uncertainty in v because (a) u is a factor of 10 larger than v, and (b) u is the velocity component that is normal to the spanwise plane. It is well known in stereo-PIV measurements that the uncertainty of the velocity component normal to the measurement plane is typically two to three times larger than velocity components measured in the plane. The mean uncertainty for v is about twice the estimate of the repeatability uncertainty quoted above (Sec. B). Note that even though the w velocity component is normal to the streamwise plane, its mean uncertainty is slightly smaller than the v component. The v component is the only component that occurs in both the streamwise and spanwise planes.

A similar set of residual plots was generated for each of the measured quantities of interest. Here we only show three samples of these results. Figure 6(a) shows the residuals of the streamwise normal stress $< u'^2 > /U_\infty^2$ versus the normal stress measured at the intersection of each of the planes. Here we observe an increase in the uncertainty as a function of the magnitude of the stress. This type of scatter plot for uncertainty can be represented as a linear regression function. We require that the linear regression pass through (0, 0) so that the only parameter that is computed is the slope of the line.

Figure 6(b) shows the residuals in the transverse normal stress $< v'^2 > /U_\infty^2$ versus the magnitude of the average values of $< v'^2 > /U_\infty^2$ in each plane. Here we have a similar linear function to that seen for $< u'^2 > /U_\infty^2$. The linear regression indicates that both the uncertainties in $< u'^2 > /U_\infty^2$ and $< v'^2 > /U_\infty^2$ increase with their magnitude. The slope gives an indication of relative magnitude of the uncertainty with respect to the value of the quantity and can be converted into a percentage. We see then that this indicates the uncertainty in $< u'^2 > /U_\infty^2$ relative to its magnitude is just under 20%, while for $< v'^2 > /U_\infty^2$ it is just under 40%. Figure 6(c) shows $< u'v' > /U_\infty^2$ versus the average of $< u'v' > /U_\infty^2$ measured in each planes. It is not clear that the data support the idea of a linear variation for $< u'v' > /U_\infty^2$, but if a similar relationship were assumed it would be of like magnitude. It is important to state that this level of uncertainty in turbulence quantities provides a good qualitative measure for turbulence modelers.

Table 2 summarizes the results of the statistical uncertainty estimation for a number of quantities of interest. For quantities of interest that show no clear trend of the scatter plot, the table shows values for the mean and standard deviation of the residuals. For quantities that show a linearly increasing trend of the uncertainty, the table shows the value of the slope of the linear regression ($Y = a + bX$). We are still analyzing the results to try and explain why certain quantities have a linear trend and some do not. Values of uncertainty (the mean of the residuals) that are given in the table are used for the experimental uncertainty when comparing CFD results with the UMich. data.

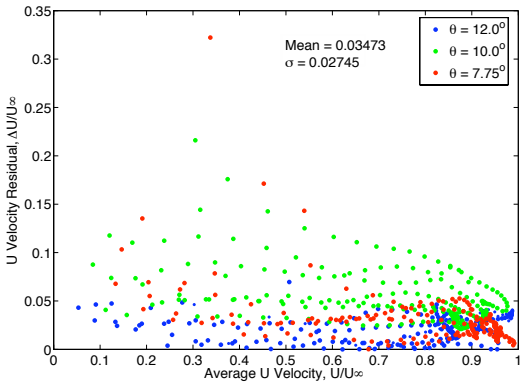

(a) Streamwise velocity, u/U_∞

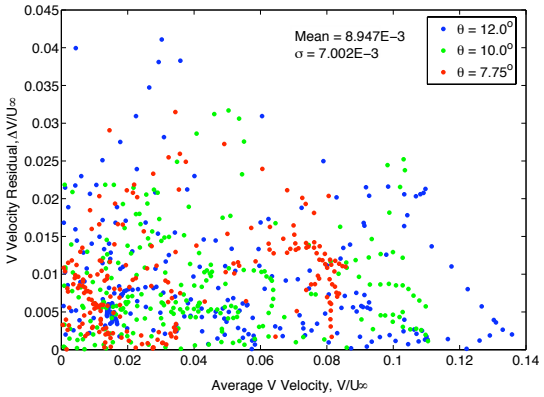

(b) Transverse velocity, v/U_∞

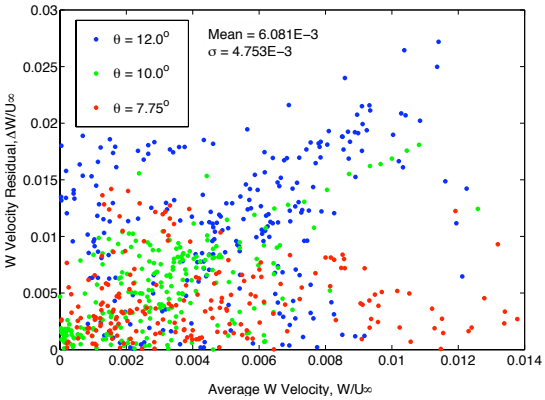

(c) Spanwise velocity, w/U_∞

Figure 5. Residuals of multiple measurements velocity and mean velocity components from the UMich. experiment

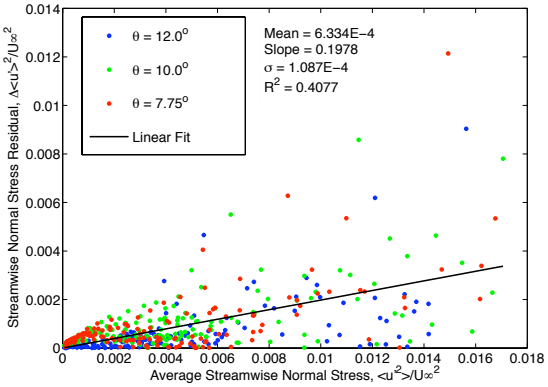

(a) Streamwise normal stress, $< u'^2 > /U_\infty^2$

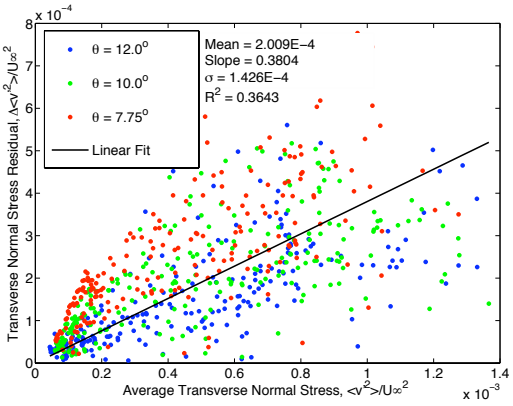

(b) Transverse normal stress, $< v'^2 > /U_\infty^2$

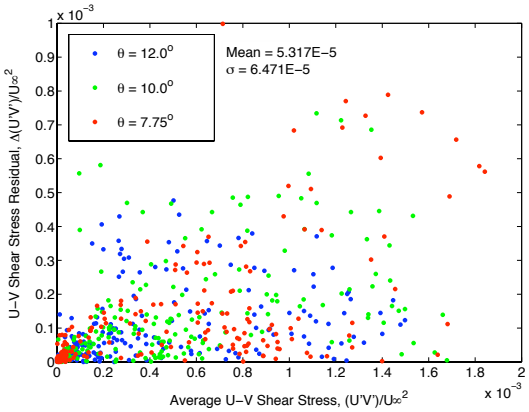

(c) Shear stress, $< u'v' > /U_\infty^2$

Figure 6. Residuals of turbulent stresses versus the average stress measured in each plane from the UMich. experiment

	u/U_∞	v/U_∞	w/U_∞	$< u'^2 > /U_\infty^2$	$< v'^2 > /U_\infty^2$	$< u'v' > /U_\infty^2$
mean uncertainty	0.03473	0.008947	0.006081	$6.334 \cdot 10^{-4}$	$2.009 \cdot 10^{-4}$	$5.317 \cdot 10^{-5}$
std. dev. of the uncertainty	0.02745	0.007002	0.004753	0.001087	$1.426 \cdot 10^{-4}$	$6.471 \cdot 10^{-5}$
linear regression slope, b				0.1978	0.3804	

Table 2. Summary of the statistical uncertainty analysis

IV. CFD Solutions

Eleven individuals from nine different organizations submitted solutions to the workshop for evaluation. Table 3 summarizes the submissions. The solutions were from both Reynolds Averaged Navier-Stokes (RANS) methods and unsteady Navier-Stokes methods, which we will classify here as large-eddy simulation (LES). The RANS methods employed a variety of turbulence models and the LES methods used a variety of sub-grid models and numerical schemes. Both structured and unstructured grid methods were employed.

Name	Organization	Code	Method	Turbulence Model
Baurle	NASA Langley	Vulcan	RANS	Menter BSL
Baurle	NASA Langley	Vulcan	RANS	Menter SST
Baurle	NASA Langley	Vulcan	RANS	$k-\omega$
Baurle	NASA Langley	Vulcan	RANS	$k-\omega$ + Durbin correction
Bhagwandin	Army Research Lab	CFD++	RANS	Realizable $k-\epsilon$
Bhagwandin	Army Research Lab	CFD++	RANS	Spalart-Almaras
Bhagwandin	Army Research Lab	CFD++	RANS	Menter SST
Duraisamy	Stanford Univ.	Joe	RANS	Menter SST
Edwards	North Carolina State Univ.		LES	
Edwards	North Carolina State Univ.		RANS	Menter SST
Georgiadis	NASA Glenn	Wind-US	RANS	Menter SST
Jamalamadaka	Michigan State Univ.		LES	
Park[15]	NASA Langley	FUN3D	RANS	Spalart-Almaras
Pirozzoli[16]	Univ. Roma		LES	
Rumsey	NASA Langley	CFL3D	RANS	Spalart-Almaras
Subbareddy	Univ. of Minnesota	US3D	LES	IDDES
Tapee	Northrup-Grumman	RANS		

Table 3. Summary of the submitted solutions

The majority of RANS submissions modeled the entire wind tunnel from the nozzle plenum to downstream of the test section. In these cases the tunnel stagnation temperature and pressure were specified in the plenum. The LES calculations typically used a RANS simulation as an initial solution and to provide a mean inflow profile to the unsteady simulation of the test section. The LES solutions also required a fluctuating component to the inflow profile. This was obtained through boundary layer recycling techniques, precursor simulations or theoretical means.

Each analyst was responsible for post-processing their solutions. This included interpolating their solutions onto the experimental measurement grids and ensuring that the quantities were provided in the proper dimensional form. The analysts were free to choose which cases to run and what data to provide. A total of 36 solutions were provided and 21 included the turbulent stresses.

A. Description of the Error Metric

In order to objectively evaluate the submitted solutions an error metric, E, was defined. The validation metric is a simple average of the magnitude of the difference between the CFD and experiment at every point in a measurement plane. The metric is expressed as

$$E(f) = \frac{1}{N}\sum_{n=1}^{N}\left|(f_{cfd})_n - (f_{exp})_n\right| \tag{1}$$

For the error in velocities the metric is nondimensionalized by the freestream velocity, U_∞. For the error in the turbulence shear stress the metric is nodimensionalized by the square of the freestream velocity, U_∞^2. The IUSTI normal stresses ($\sqrt{< u'^2 >}$ & $\sqrt{< v'^2 >}$) are nondimensionalized by U_∞ and the UMich normal stresss ($< u'^2 >$ & $< v'^2 >$) are nomdimensionalized by U_∞^2 For a detailed discussion of the construction and use of validation metrics see Ref.[11]

B. Examination of Representative Solutions

The error metric was computed for all the measured variables and all solutions. In the interest of brevity, the comparisons shown here are limited to streamwise and transverse velocities as well as turbulent stresses. The velocity derivatives from the UMich experiment were computed using the experimentally obtained velocities and differenced on the PIV measurement grid. They do not provide any additional information for comparison beyond the velocity data and are a poor comparison to the CFD because the CFD derivatives were computed on their own grids, which are much finer. The spanwise velocity, w/U_∞, is also a poor quantity for comparison to CFD on the centerline. The tunnel geometry is symmetric about this plane. The experimental data reveals that the spanwise velocity was not zero, indicating asymmetry in the flow. CFD can not reliably predict such asymmetries and in almost all cases will produce symmetric solutions (in many cases symmetry was specified in the computation) with zero spanwise velocity.

Because the streamwise velocity, u/U_∞, is the dominant component most of the attention will be focused on it. First, the general characteristics of the flowfields and the error metrics will be presented. For each case, the solutions with the lowest ("best") and highest ("worst") measure of error in streamwise velocity, $E(u)/U_\infty$ will be shown.

C. IUSTI Mach 2.25 – 8.0 degree case

Figure 7 compares contours of streamwise velocity for the experiment and the best and worst CFD predictions of the IUSTI Mach 2.25, $\theta = 8.0°$ case. For this case, the measurement plane extends vertically only to the edge of the interaction. The shock wave is not visible. The flow separates from the wall and the boundary layer downstream of the separation bubble is significantly thicker. The best solution appears very similar to the experiment, although the size of the separation bubble and downstream boundary layer are slightly under-predicted. The worst solution shows a much smaller separation and thinner downstream boundary layer. Fig. 8 shows the contours of the error metric for the streamwise velocity. The error contours clearly show the regions where the predictions deviate from the PIV data. The regions of high error are concentrated near the separation bubble. The maximum error in the best solution is approximately $0.2U_\infty$, while the maximum error in the worst solution is near $0.35U_\infty$. A more traditional comparison is shown in Fig. 9 where velocity are given at several streamwise locations. Error bars based on the experimentalists' estimate[5] are included on the PIV data, but are within the size of the symbols representing the data. Despite the fact that the PIV method can not measure very near the wall, it is seems apparent from the profiles that the best solution should do a much better job of predicting quantities of interest such as skin friction.

D. UMich. Mach 2.75 – 7.75, 10.0 and 12.0 degree cases

Figure 10 compares contours of streamwise velocity for the experiment and the best and worst CFD predictions of the UMich Mach 2.75, $\theta = 7.75°$ case. For the Michigan cases, the measurement plane extends beyond the interaction to include a portion of the freestream flow. The shock wave is visible, but appears smeared in the data. This smearing could be due to some unsteadiness in the shock position and/or the volume-averaging nature of the PIV technique. It is not clear if the flow is separated. Both CFD solutions under-predict the size of the interaction region and downstream boundary layer thickness. Fig. 11 shows the

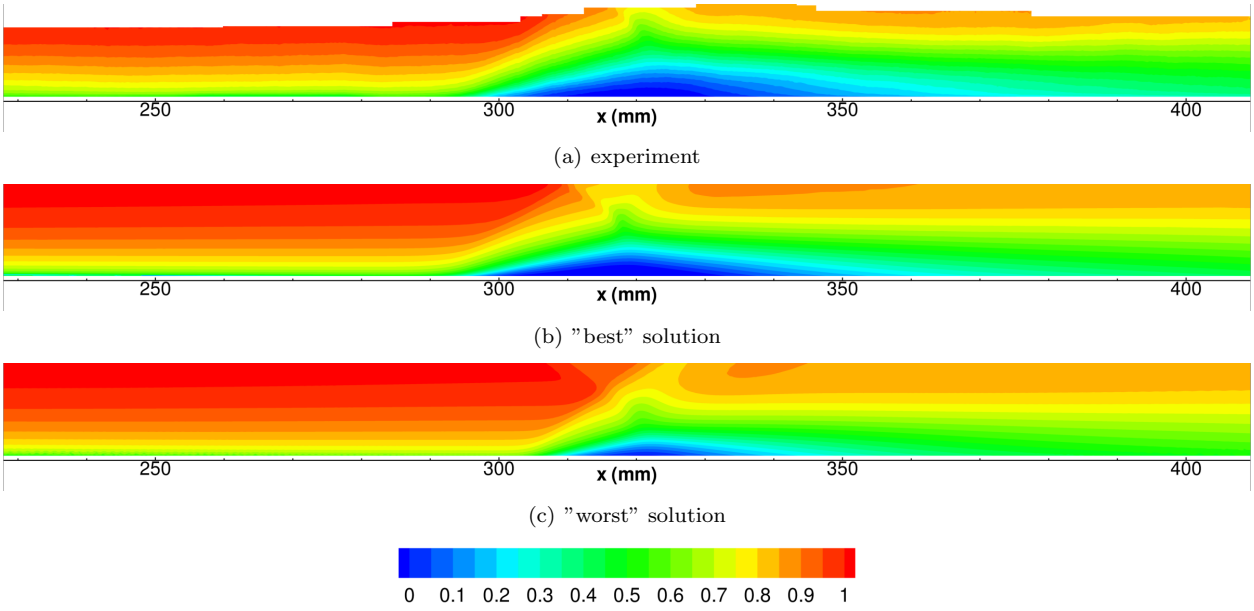

(a) experiment

(b) "best" solution

(c) "worst" solution

Figure 7. IUSTI $M = 2.25$ $\theta = 8.0°$, contours of streamwise velocity, u/U_∞

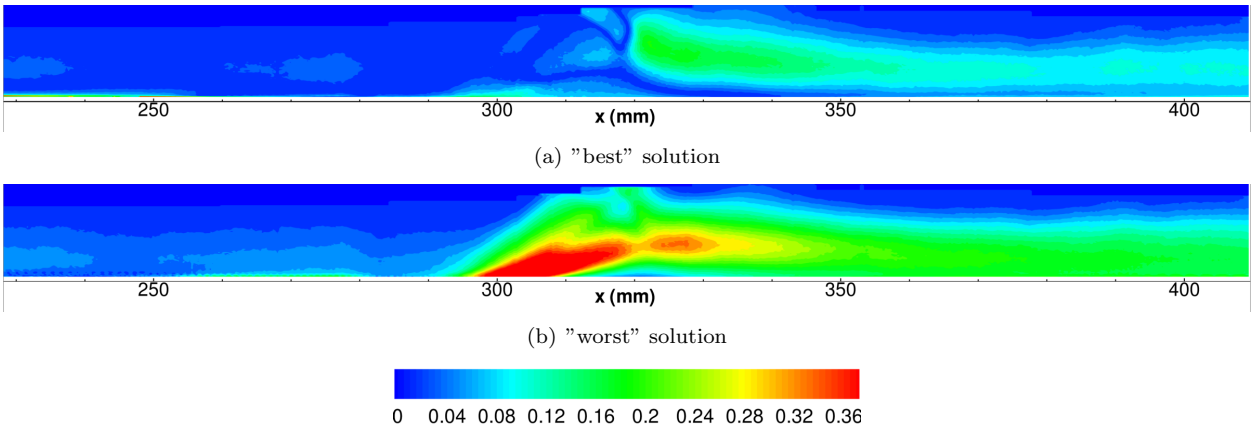

(a) "best" solution

(b) "worst" solution

Figure 8. IUSTI $M = 2.25$ $\theta = 8.0°$, contours of streamwise velocity error, $E(u)/U_\infty$

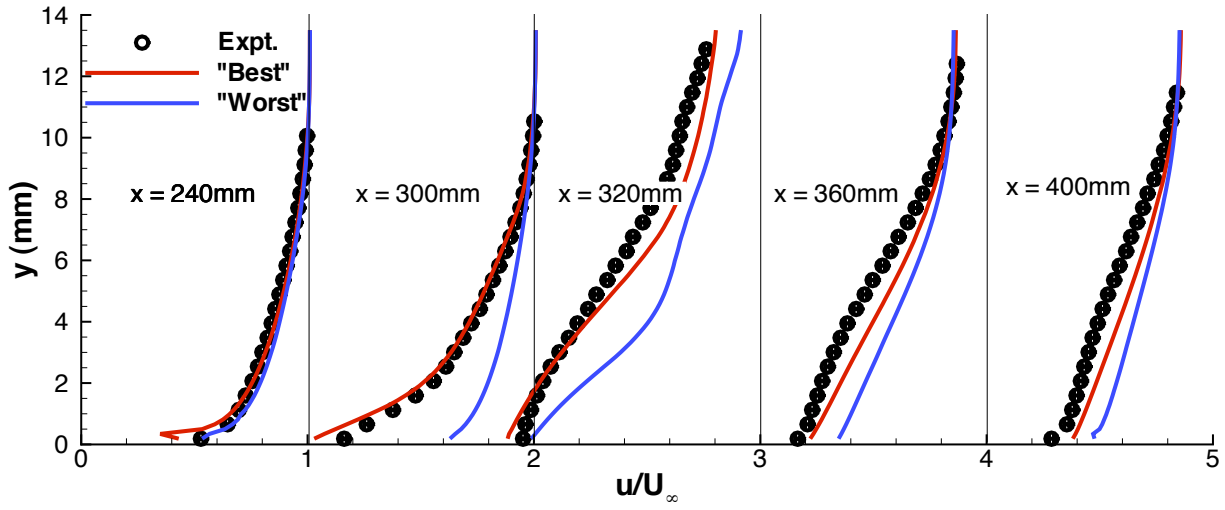

Figure 9. IUSTI $M = 2.25$ $\theta = 8.0°$, streamwise velocity profiles, u/U_∞

contours of the error metric for the streamwise velocity. In addition to the error in the interaction region, the plots show some error in the location of the shock wave and its reflection. The maximum error in the best solution is approximately $0.13U_\infty$, while the maximum error in the worst solution is near $0.27U_\infty$. Velocity profiles are shown in Fig. 12. Error bars based on the analysis in this paper are included on the PIV data. Equivalent figures for the UMich $\theta = 10.0°$ and $\theta = 12.0°$ are shown in Figs. 13 - 15 and 16 - 18. The interaction grows larger with increasing deflection angle and the error levels increase for both the best and worst predicted solutions.

E. Prediction of Turbulent Stresses

The turbulent stresses are computed very differently depending on the numerical approach used. For the RANS solutions submitted, the stresses are not explicitly computed and must be derived from the turbulence model variables. Typically the Boussinesq approximation is used to compute the components of the stress tensor based on the turbulent kinetic energy from a two-equation model. In the case of a one-equation turbulence model, an additional approximation for turbulent kinetic energy must be made. An example of how this may be done is given by Georgiadis et al.[17] For the LES methods, the stresses are computed directly in the simulation. Because the LES solutions have less reliance on modeling approximations, one can expect that they will yield better results.

Two predictions for the turbulent stresses were submitted for the IUSTI case, one RANS and one LES. The solutions are compared with the experiment in Figs. 19 - 21. The experimental data shows very high levels of streamwise normal stress in the forward portion of the interaction region. This feature is predicted well by the LES and missed by the RANS (Fig. 19).

The experiment shows that the form and levels of the transverse normal stress differ significantly from the streamwise normal stress. The LES solution depicts this change accurately. The RANS prediction of the two normal stresses are very similar. This deficiency in the RANS prediction is a direct consequence of the approximate method necessary to derive the stresses from the turbulence model.

The shear stress is shown in Fig. 21. Here, the RANS solution is much improved. The improved prediction of the shear stress for RANS is not surprising. RANS turbulence models directly affect the solution through the shear stress term in the equations and the models are developed and tuned to accurately model this term.

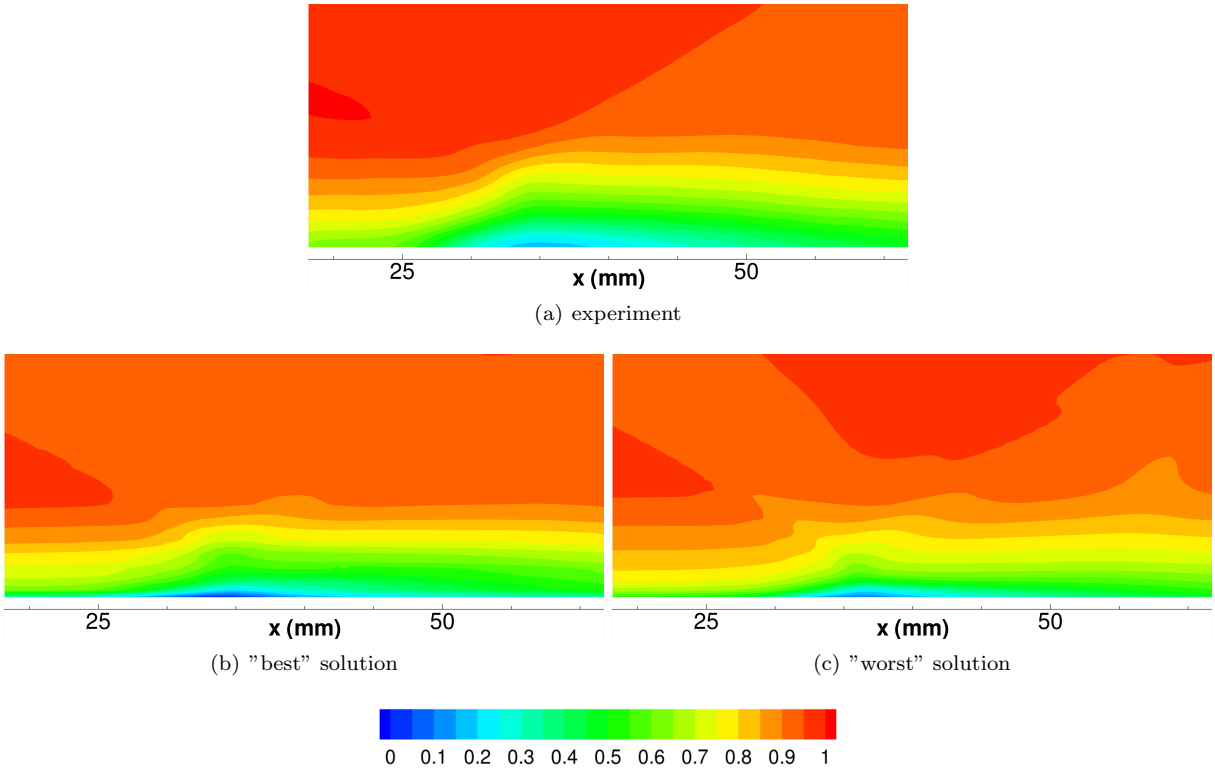

(a) experiment

(b) "best" solution

(c) "worst" solution

Figure 10. UMich. $M = 2.75$ $\theta = 7.75°$**, contours of streamwise velocity,** u/U_∞

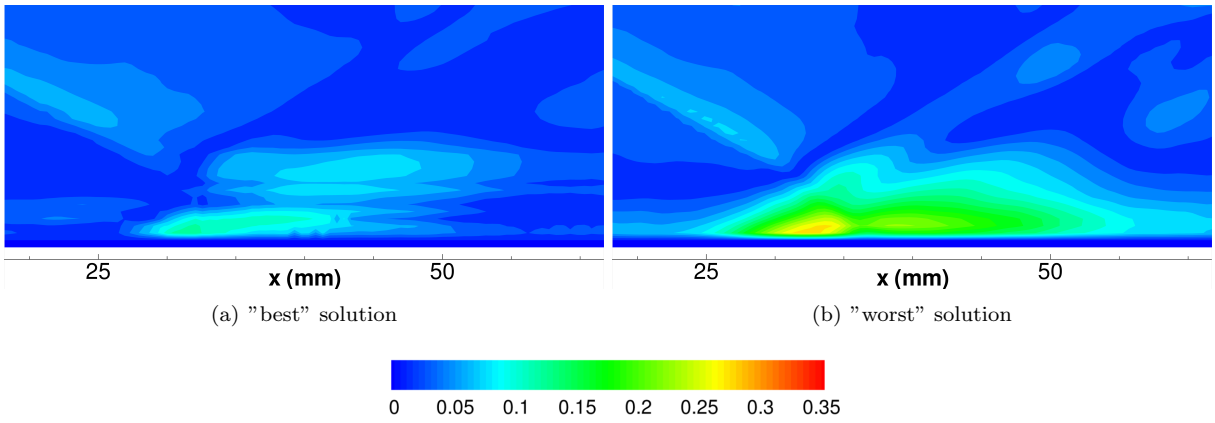

(a) "best" solution

(b) "worst" solution

Figure 11. UMich. $M = 2.75$ $\theta = 7.75°$**, contours of streamwise velocity error,** $E(u)/U_\infty$

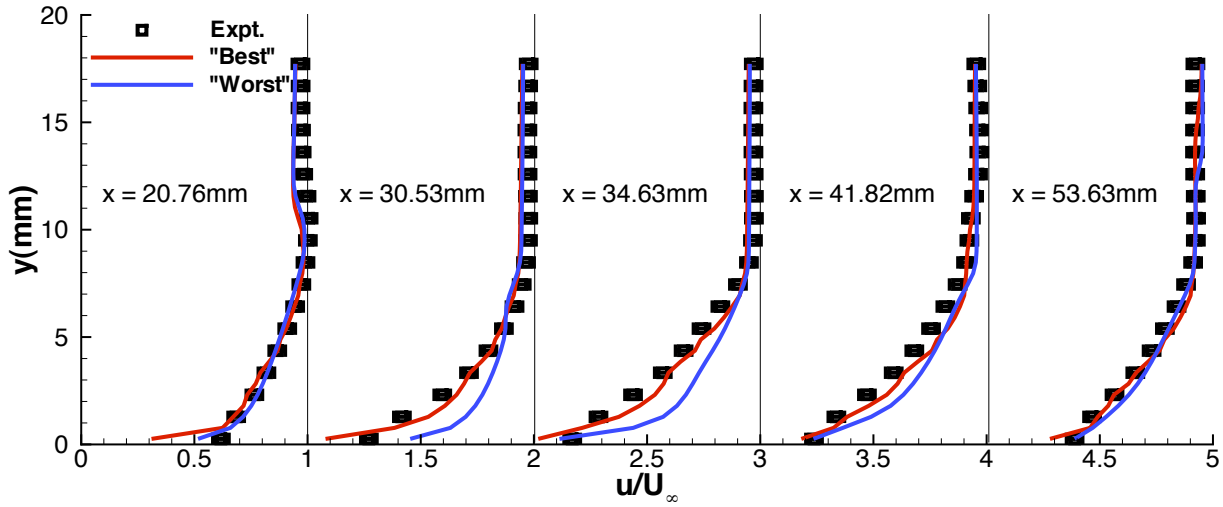

Figure 12. UMich. $M = 2.75$ $\theta = 7.75°$**, streamwise velocity profiles,** u/U_∞

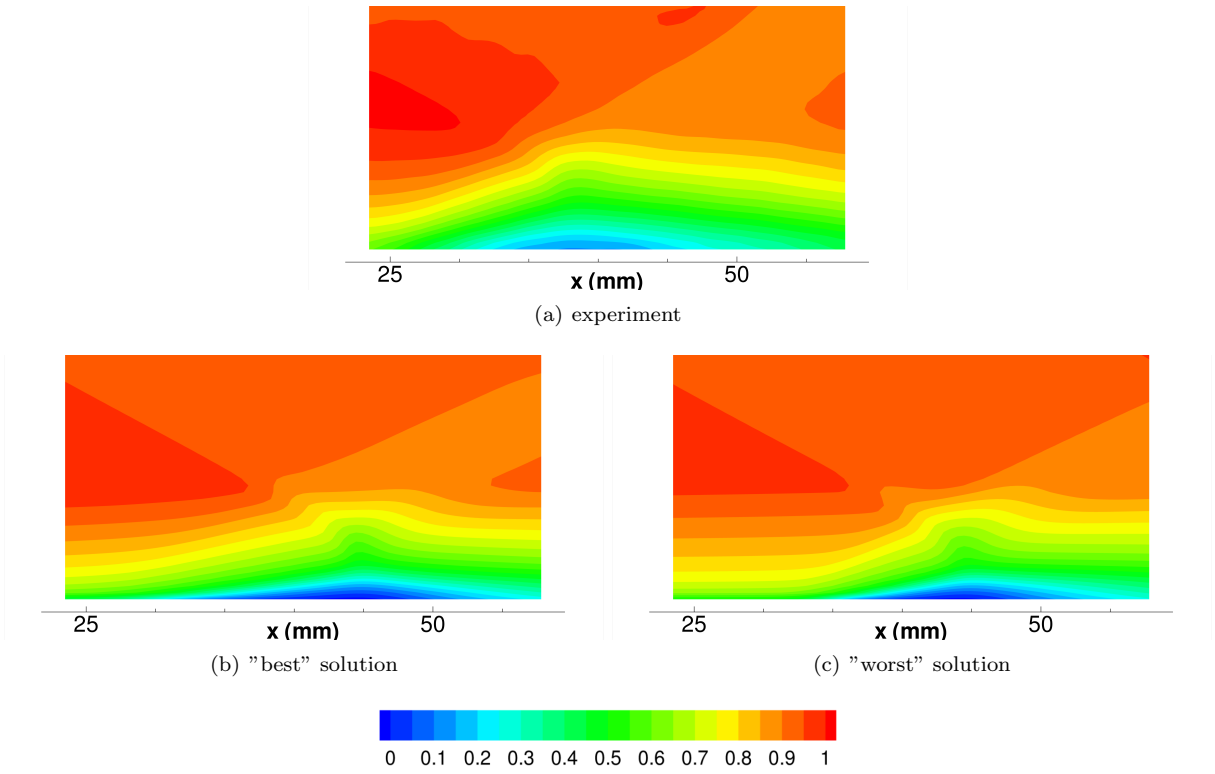

(a) experiment

(b) "best" solution

(c) "worst" solution

Figure 13. UMich. $M = 2.75$ $\theta = 10.0°$**, contours of streamwise velocity,** u/U_∞

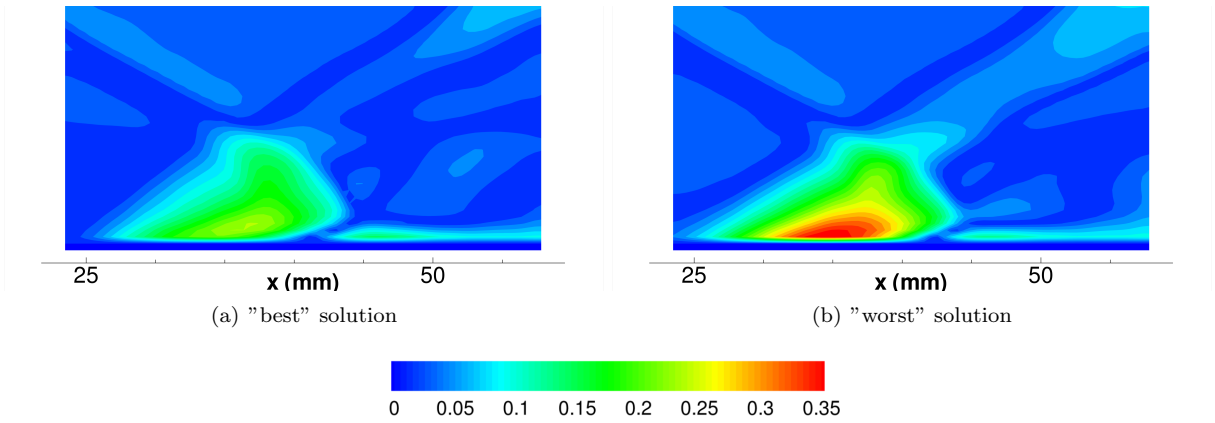

(a) "best" solution (b) "worst" solution

Figure 14. UMich. $M = 2.75$ $\theta = 10.0°$**, contours of streamwise velocity error,** $E(u)/U_\infty$

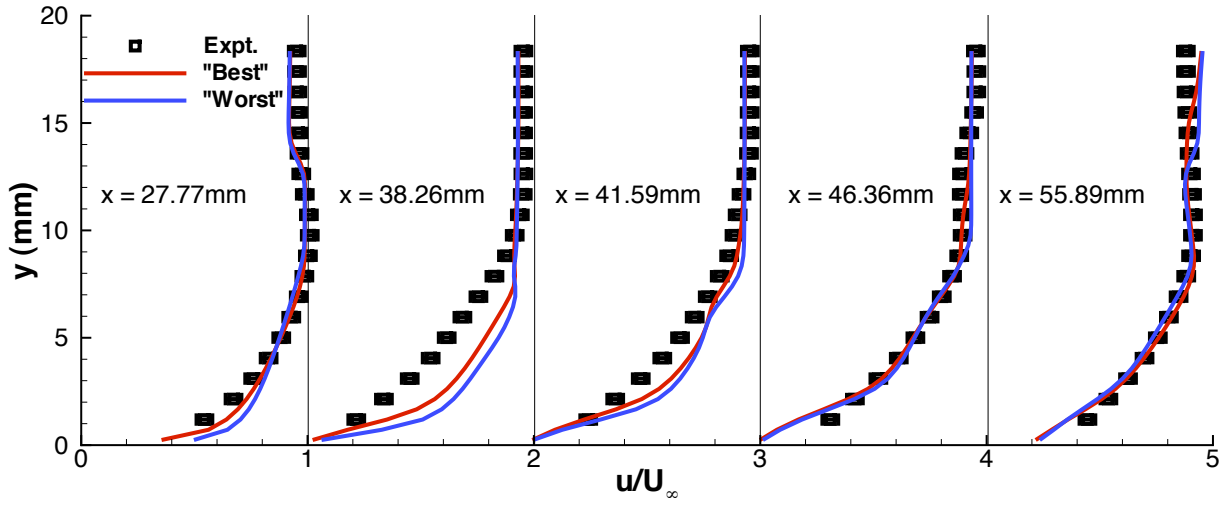

Figure 15. UMich. $M = 2.75$ $\theta = 10.0°$**, streamwise velocity profiles,** u/U_∞

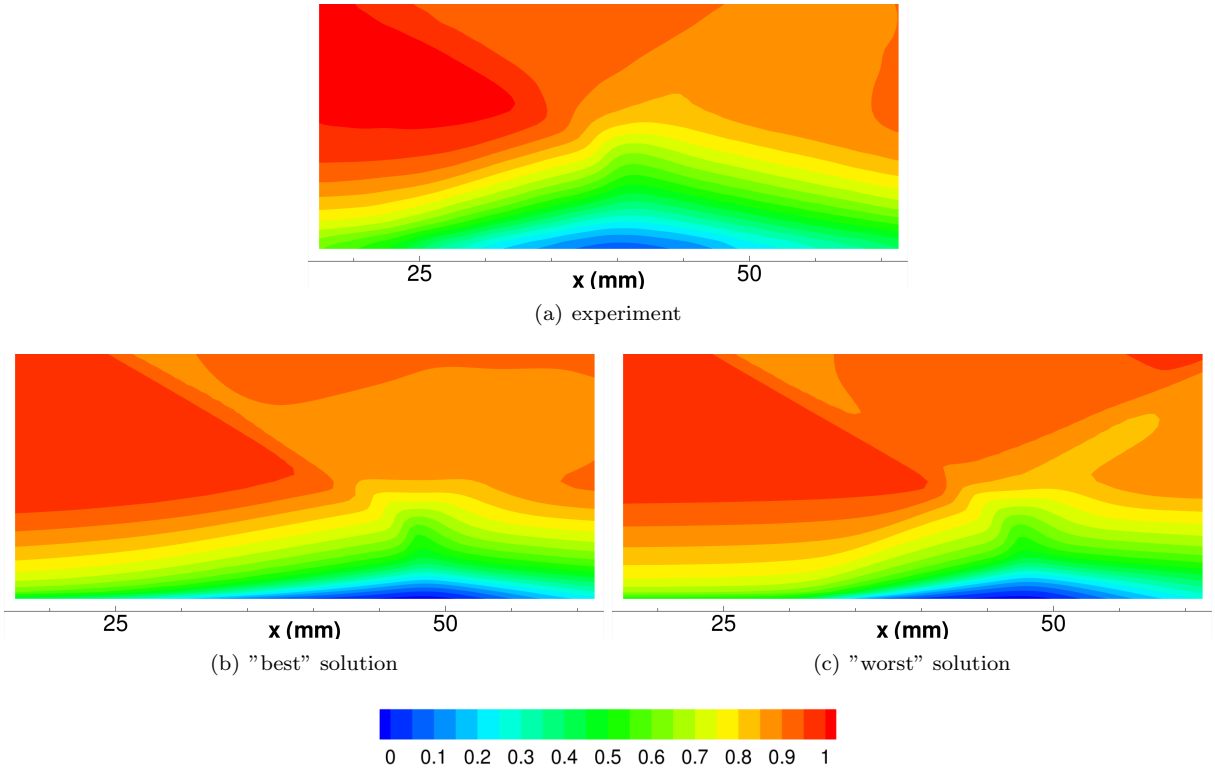

(a) experiment

(b) "best" solution

(c) "worst" solution

Figure 16. UMich. $M = 2.75$ $\theta = 12.0°$**, contours of streamwise velocity,** u/U_∞

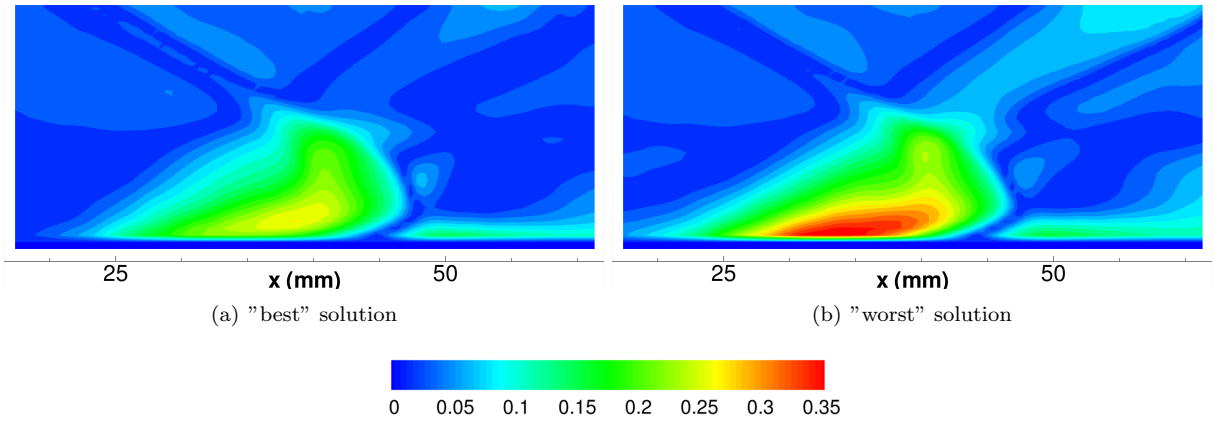

(a) "best" solution

(b) "worst" solution

Figure 17. UMich. $M = 2.75$ $\theta = 12.0°$**, contours of streamwise velocity error,** $E(u)/U_\infty$

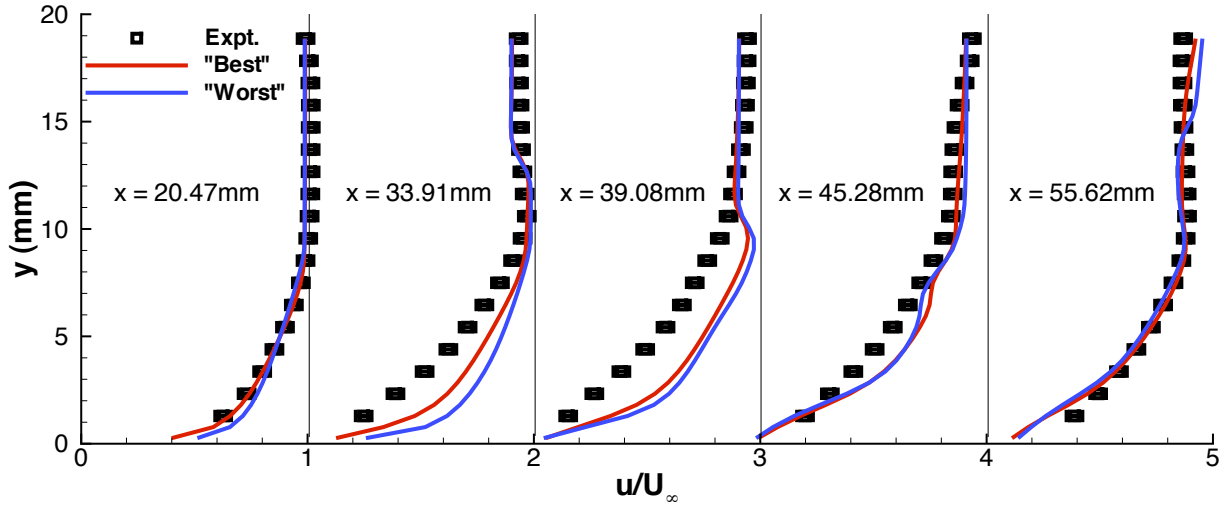

Figure 18. UMich. $M = 2.75$ $\theta = 12.0°$**, streamwise velocity profiles,** u/U_∞

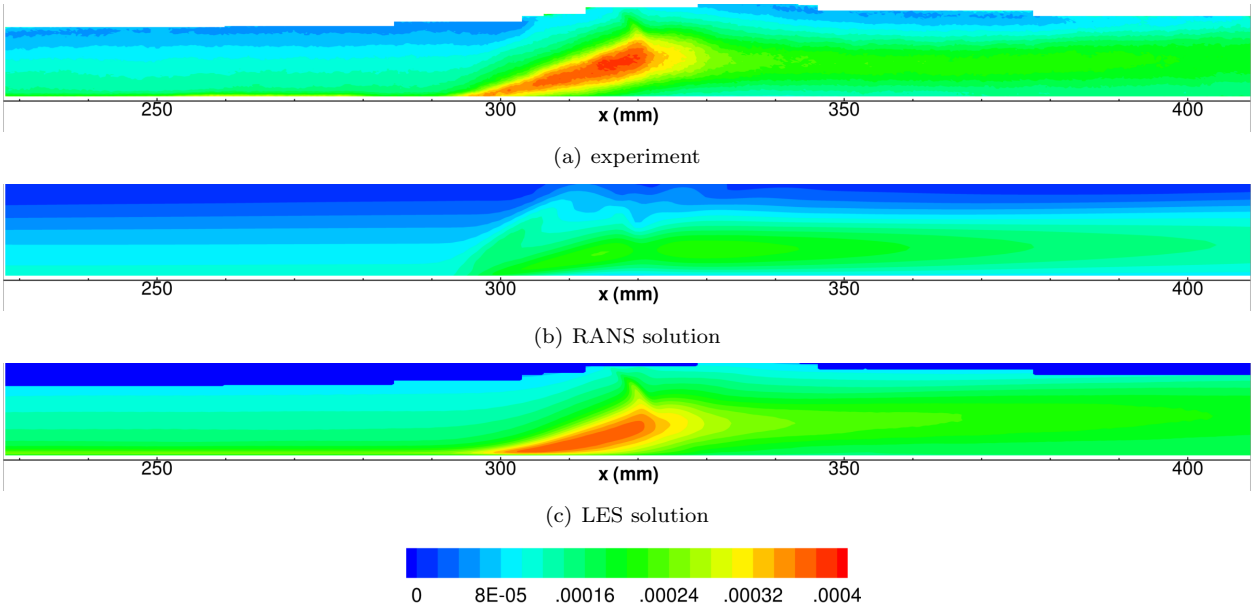

(a) experiment

(b) RANS solution

(c) LES solution

Figure 19. IUSTI $M = 2.25$ $\theta = 8.0°$**, contours of streamwise normal stress,** $\sqrt{< u'^2 >}/(U_\infty)^2$

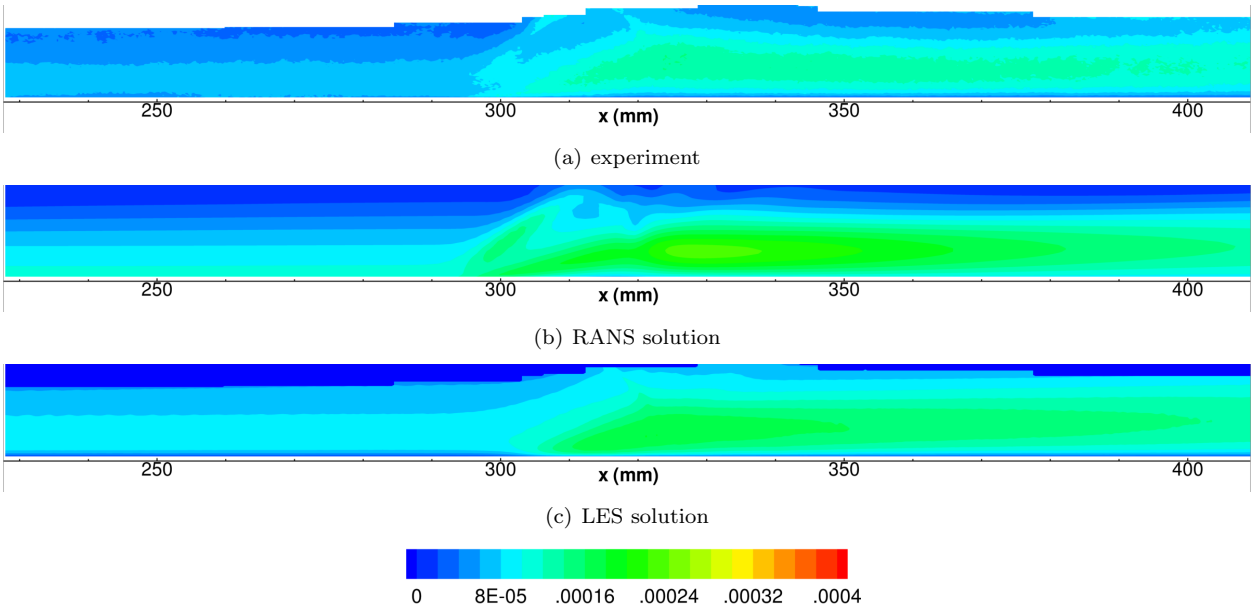

(a) experiment

(b) RANS solution

(c) LES solution

Figure 20. IUSTI $M = 2.25$ $\theta = 8.0°$, contours of transverse normal stress, $\sqrt{< v'^2 >}/(U_\infty)^2$

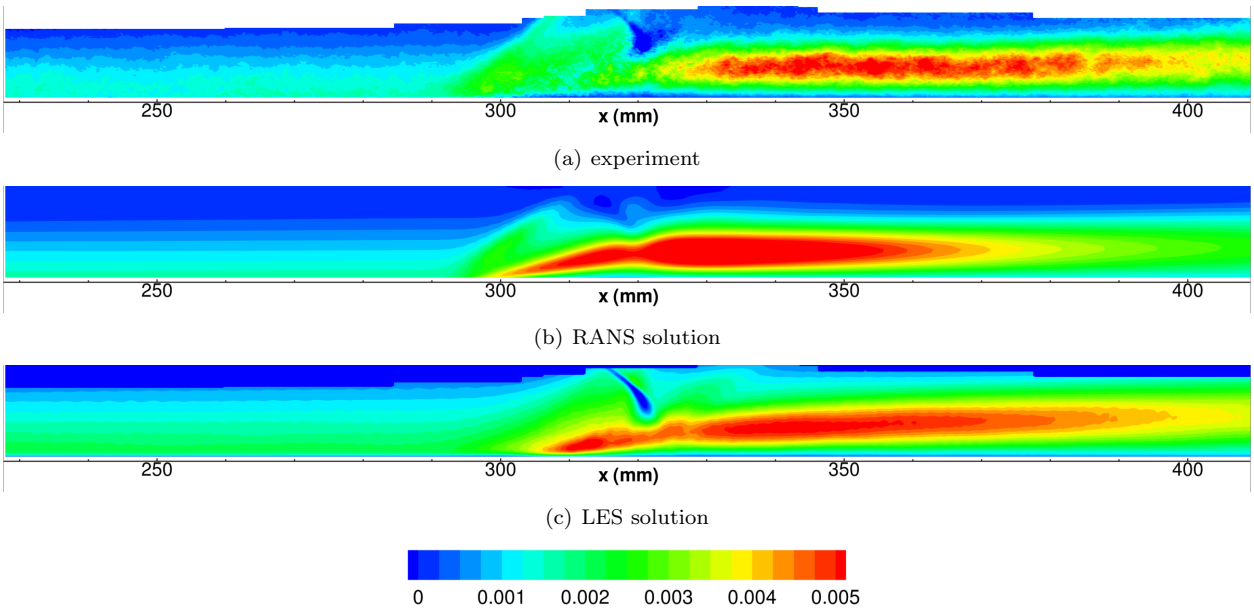

(a) experiment

(b) RANS solution

(c) LES solution

Figure 21. IUSTI $M = 2.25$ $\theta = 8.0°$, contours of shear stress, $- < u'v' > /(U_\infty)^2$

F. Comparison of all Solutions

1. *IUSTI, Mach 2.25, $\theta = 8.0$*

The error for all seven predictions (denoted A through G) of the IUSTI case are shown in Fig. 22. For the velocity components, the experimental uncertainty quoted by the experimentalists, 1.1 percent of freestream velocity, is represented by the dashed line. The average error in streamwise velocity for the CFD predictions ranged between 3.8 and 9.0 percent of freestream velocity, which is well above the experimental error. The errors in transverse velocity are all near the experimental uncertainty. The relative accuracy of the methods is not consistent between the variables plotted here. For example, submission F provides the lowest error in streamwise velocity, but provides the highest error in transverse velocity. The error in the prediction of the turbulent stresses corresponds to the discussion in section E above. The LES prediction, D, does a superior job for the normal stresses and the RANS prediction, G, is better for the shear stress.

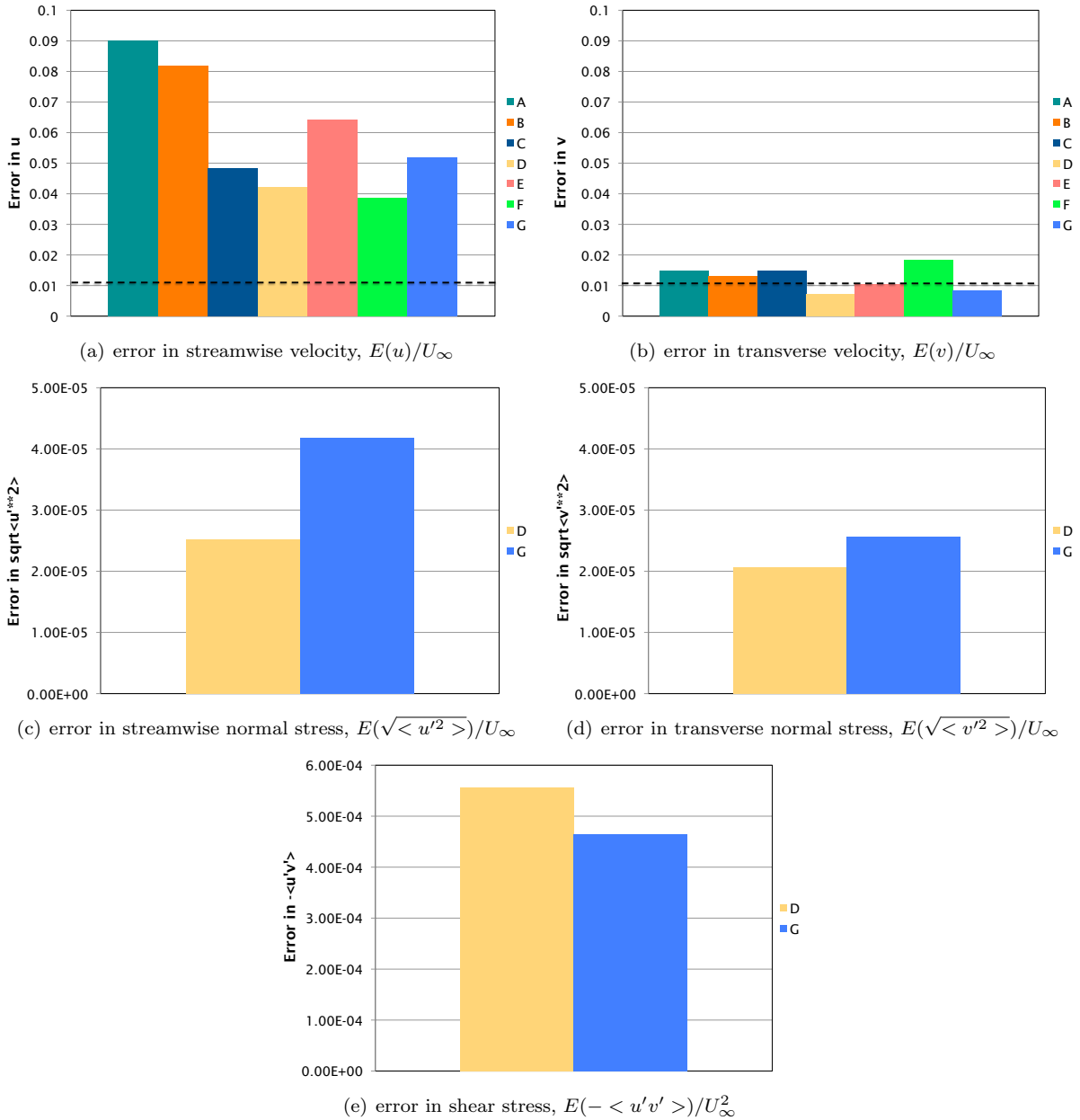

(a) error in streamwise velocity, $E(u)/U_\infty$

(b) error in transverse velocity, $E(v)/U_\infty$

(c) error in streamwise normal stress, $E(\sqrt{< u'^2 >})/U_\infty$

(d) error in transverse normal stress, $E(\sqrt{< v'^2 >})/U_\infty$

(e) error in shear stress, $E(- < u'v' >)/U_\infty^2$

Figure 22. Error assessment of the IUSTI Mach 2.25, $\theta = 8.0^\circ$ case

2. UMich. Mach 2.75 – 7.75, 10.0 and 12.0 degree cases

The errors for all predictions of the UMich., Mach 2.75 cases are shown in Figs. 23 - 25. The experimental uncertainties from the statistical estimation are represented by the dashed lines. For the turbulent normal stresses, the mean uncertainty was used, which represents the uncertainty in all planes. A better estimate for a given plane could be made using the linear regression and integrating the product of the slope and measured value of the stress over that plane. All of the CFD predictions of streamwise velocity and streamwise normal stress are near (many are below) the levels of the experimental uncertainty. This suggests that any conclusions based on the error data are not valid. But as shown in Figs. 12, 15 and 18, in the interaction region the predictions lie outside of the experimental error bars suggesting that the use of this error metric with the current data can still be useful.

The computed errors in streamwise velocity for the CFD predictions are given in Table 4. The errors grow with increasing deflection angle. This is expected and is a result of the stronger shock wave, larger interaction region and more complex flowfield. The lower average errors compared to the IUSTI case is due to the inclusion of a portion of the freestream flow in the plane of interest. The freestream portion of the flow is much better predicted than the interaction region. Including this portion of the flowfield in the error calculation results in a lower average error (Figs. 11, 14 & 17).

As with the IUSTI case, there does not appear to be a correlation between prediction methodologies and the relative error for each variable examined.

Deflection Angle	Min. $E(u)/U_\infty$	Max. $E(u)/U_\infty$
7.75	0.0240	0.0404
10.0	0.0341	0.0463
12.0	0.0422	0.0581

Table 4. Minimum and maximum error in streamwise velocity for the UMich. cases

G. Discussion of Trends in the Data

In general the errors in the CFD solutions all fell within a relatively narrow band and no one method predicted all variables well. No method stood out as being clearly superior to the others. However the error contours and velocity profiles indicate that there is room for improvement in the modeling. RANS methods, such as Reynolds stress and algebraic Reynolds stress models may offer improved predictions of the turbulent stresses and other flow quantities. Also, the LES predictions suggest that as the method matures results will improve.

The submitted solutions provided a wealth of information. But, because each analyst used a different approach there are a large number of variables to consider when attempting to analyze the results. These variables include; numerical scheme, grid resolution, grid type, boundary conditions, turbulence model, gas model, etc. Based on the information that was submitted with the results and presented at the workshop an attempt was made to discern trends in the error data. This is by no means a complete analysis. And it is suggested that in order to do a more thorough study, future efforts should include submitted solutions that employ common elements such as grids, numerical schemes, etc.

1. Effect of RANS Turbulence Model

The clearest discernable effect on the solutions for the RANS submissions was that of the turbulence model. There were seven RANS methodologies that were run for all three UMich. flow cases. Fig. 26 shows the error in the streamwise velocity prediction for these submissions. For the 7.75 degree case all the Menter SST, $k-\omega$ and Spalart-Almaras model solutions are within 0.5 percent of each other. At the larger deflection angles, the error in all of the solutions increases and a clear trend is seen. All of the methods show the same relative error levels for the 10 and 12 degree cases. The $k-\omega$ models provide the lowest error and the Menter BSL model has the highest error. The Menter SST and Spalart-Almaras models produce similar error levels in between the minimum and maximum levels. For the 7.75 degree case several models also exhibit the same behavior in the relative error. The error for two Menter SST, the Spalart-Almaras and the Menter BSL

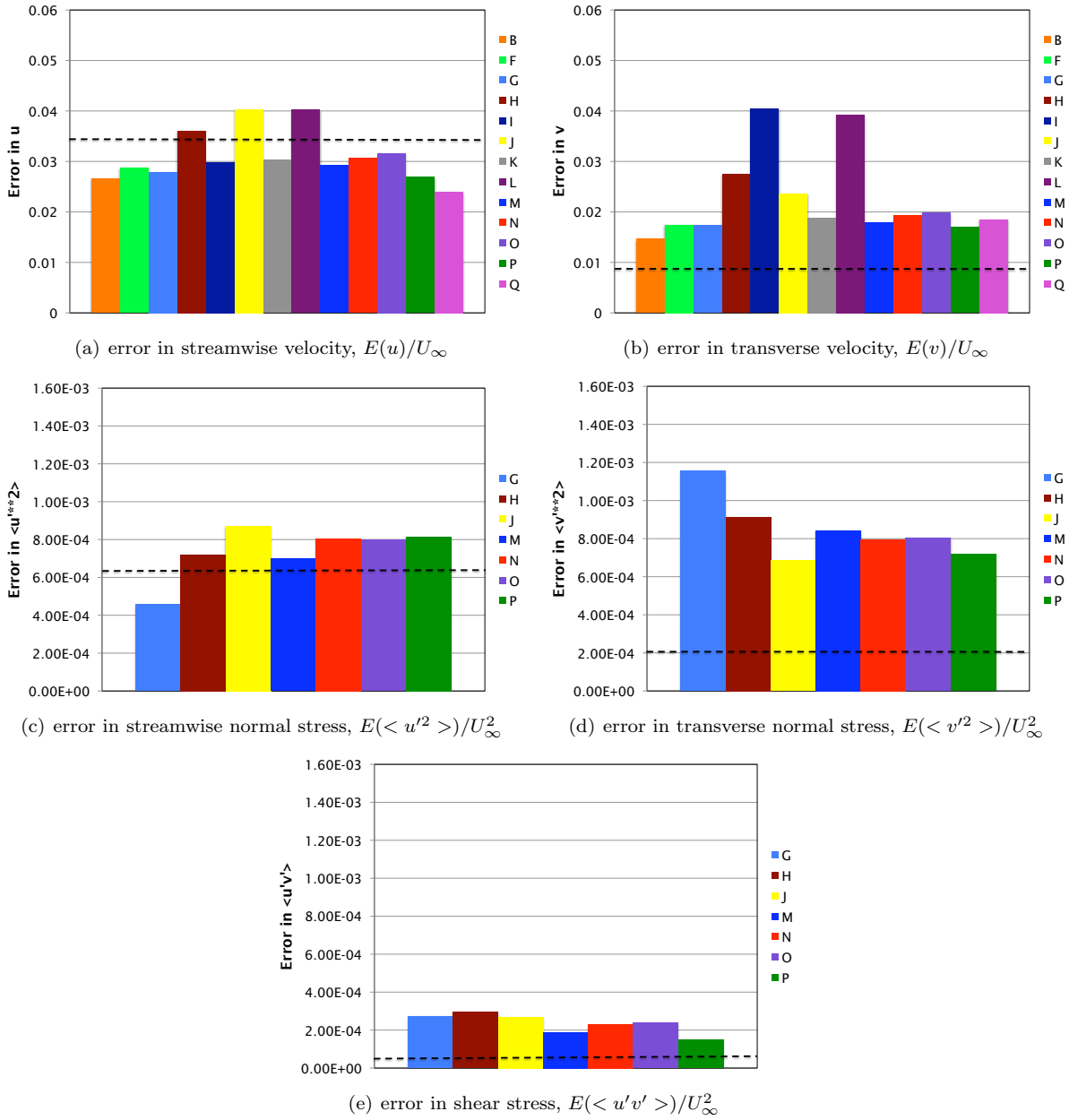

(a) error in streamwise velocity, $E(u)/U_\infty$

(b) error in transverse velocity, $E(v)/U_\infty$

(c) error in streamwise normal stress, $E(< u'^2 >)/U_\infty^2$

(d) error in transverse normal stress, $E(< v'^2 >)/U_\infty^2$

(e) error in shear stress, $E(< u'v' >)/U_\infty^2$

Figure 23. Error assessment of the UMich. Mach 2.75, $\theta = 7.75°$ case

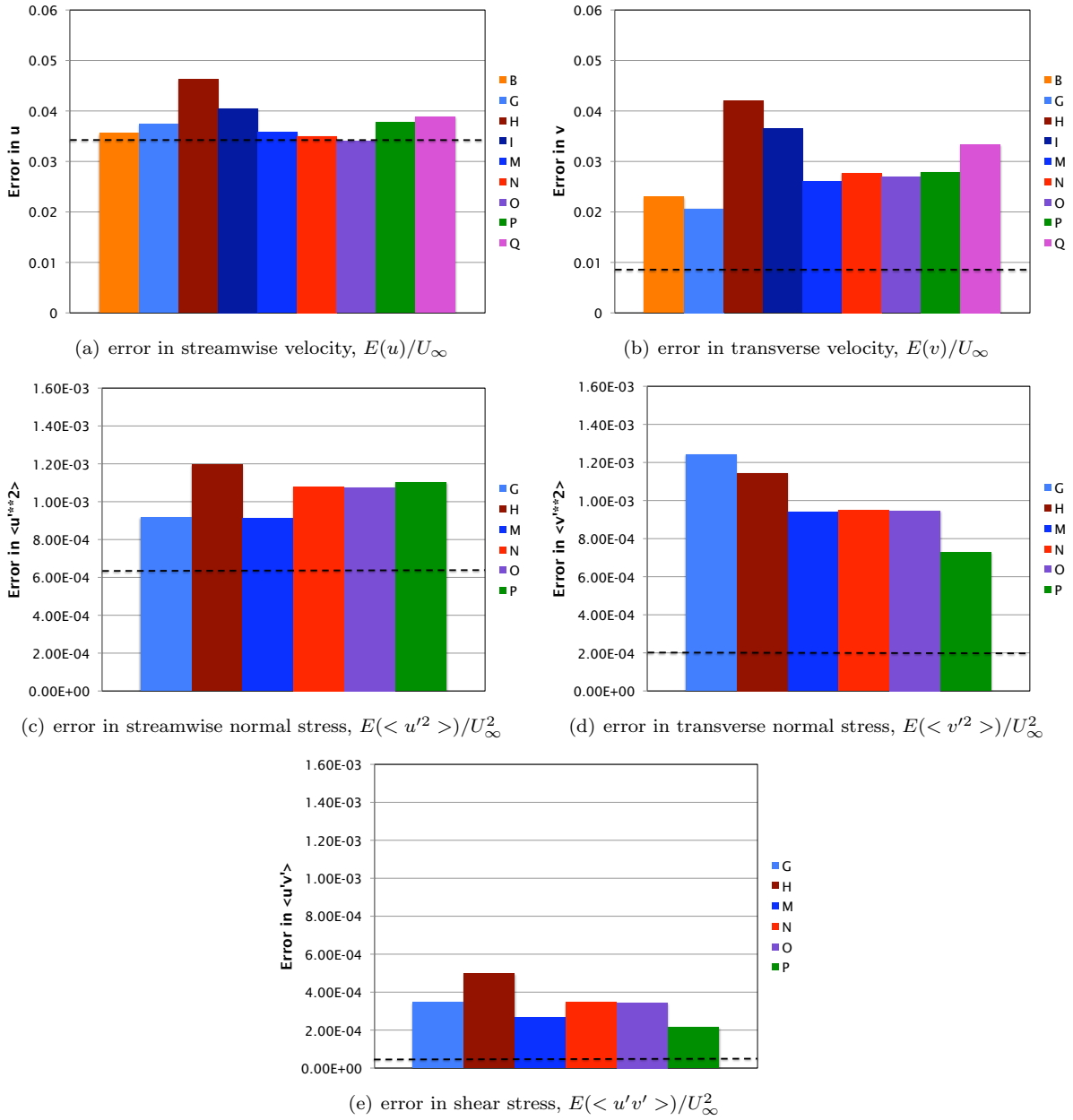

(a) error in streamwise velocity, $E(u)/U_\infty$

(b) error in transverse velocity, $E(v)/U_\infty$

(c) error in streamwise normal stress, $E(< u'^2 >)/U_\infty^2$

(d) error in transverse normal stress, $E(< v'^2 >)/U_\infty^2$

(e) error in shear stress, $E(< u'v' >)/U_\infty^2$

Figure 24. Error assessment of the UMich. Mach 2.75, $\theta = 10.0^\circ$ case

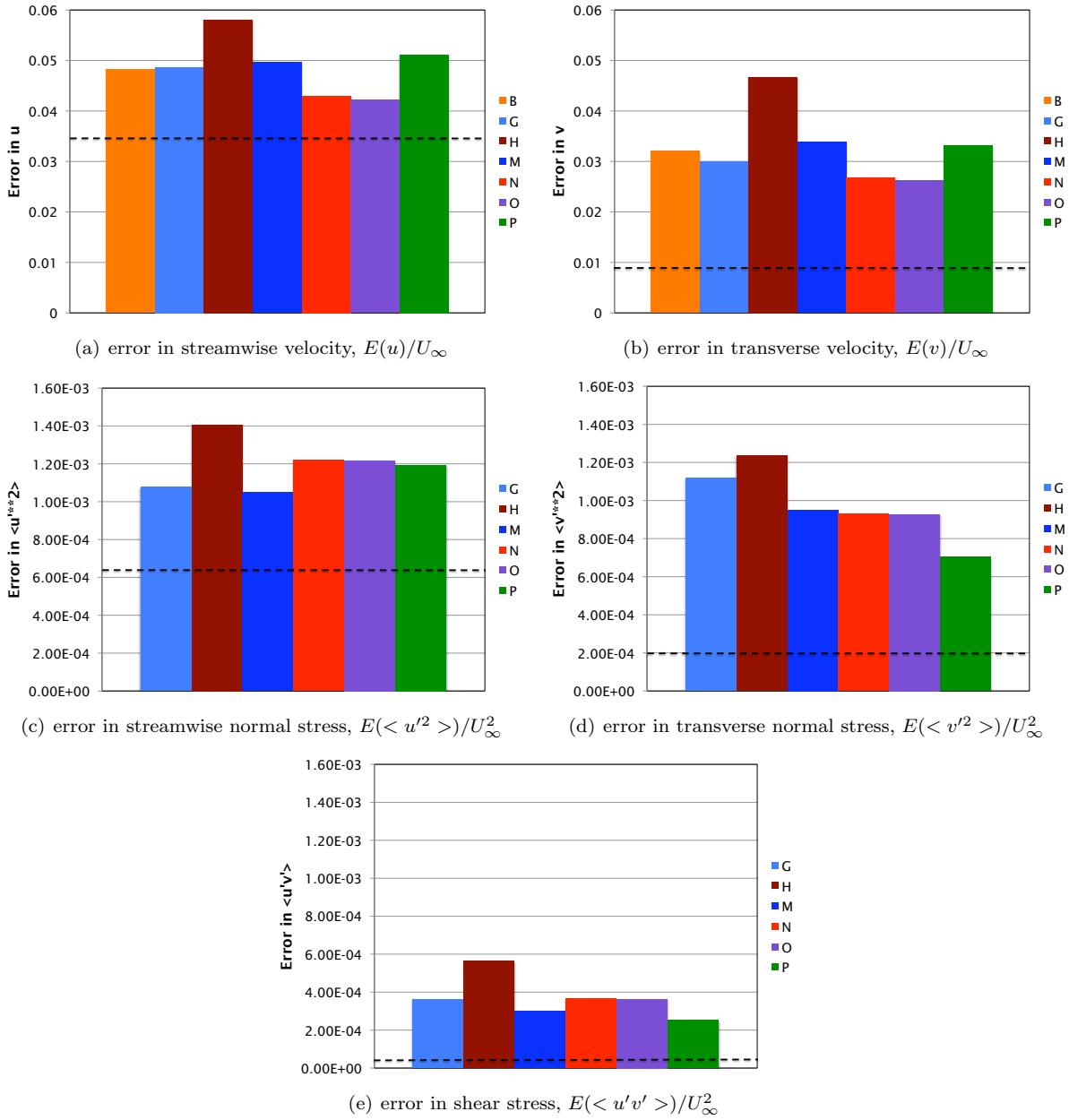

(a) error in streamwise velocity, $E(u)/U_\infty$

(b) error in transverse velocity, $E(v)/U_\infty$

(c) error in streamwise normal stress, $E(< u'^2 >)/U_\infty^2$

(d) error in transverse normal stress, $E(< v'^2 >)/U_\infty^2$

(e) error in shear stress, $E(< u'v' >)/U_\infty^2$

Figure 25. Error assessment of the UMich. Mach 2.75, $\theta = 12.0°$ case

predictions behave similarly to the 10 and 12 degree cases. The $k-\omega$ and one of the Menter SST predictions do not follow the trend.

A closer examination of the submitted solutions reveals that the predictions are strongly determined by the turbulence model used. This is illustrated by: 1) The three Menter SST solutions were from different submissions and used different grids and codes, yet there are only slight differences between them; 2) One of the Menter SST solutions, the $k-\omega$ solutions and the Menter BSL solution were all obtained using the same grid and code, illustrating a strong dependence on turbulence model.

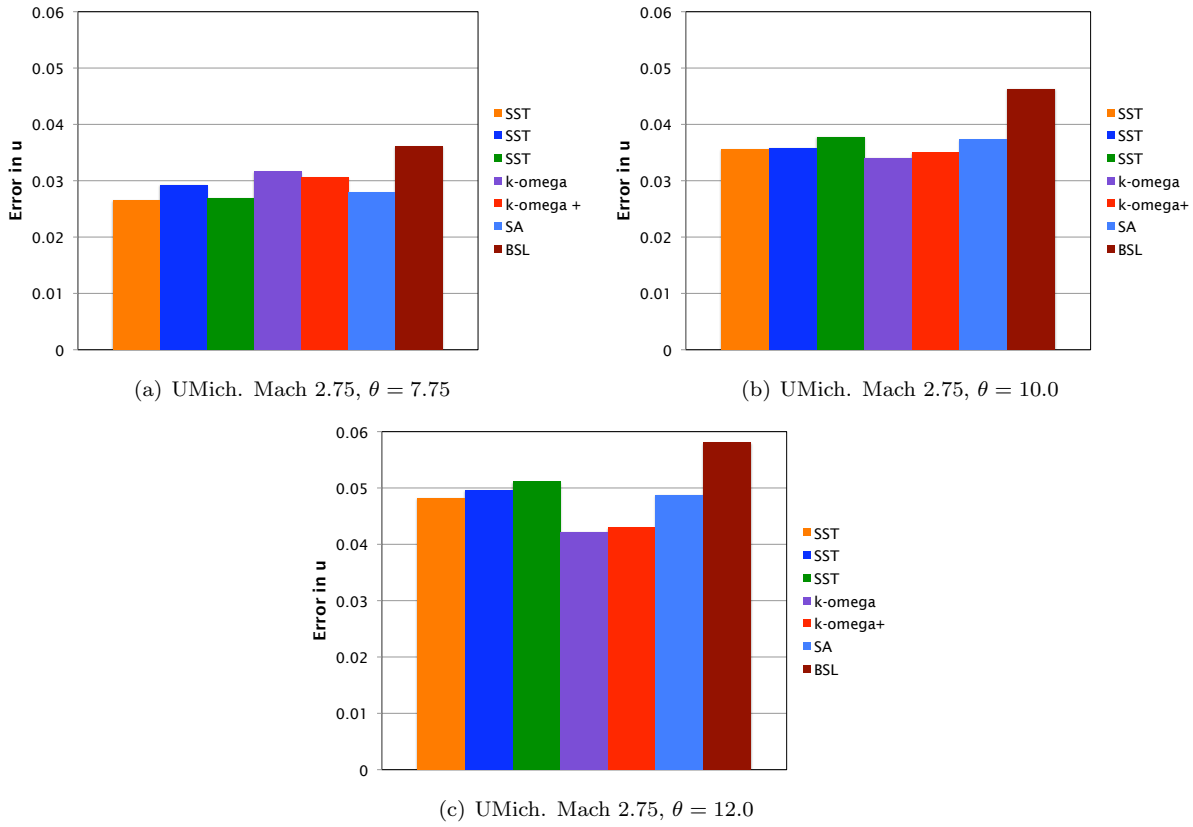

(a) UMich. Mach 2.75, $\theta = 7.75$

(b) UMich. Mach 2.75, $\theta = 10.0$

(c) UMich. Mach 2.75, $\theta = 12.0$

Figure 26. RANS turbulence model comparison for the UMich. Mach 2.75 cases. Error in streamwise velocity, $E(u)/U_\infty$

2. Effect of RANS versus LES

The UMich. Mach 2.75, $\theta = 7.75$ case was the only case where multiple LES solutions were submitted. The LES solutions were the best and worst predictions for this case. Fig. 27 shows the error levels for streamwise and transverse velocity for the best and worst RANS and LES predictions. Both methods produce very similar error levels. But because RANS methods are far more mature than LES, there is still potential for LES to provide superior predictions. In addition, if the prediction of normal stresses is important, LES should provide better accuracy.

3. Effect of Structured versus Unstructured Grids

Unstructured grid codes are widely used today. Fig. 28 shows the predictions for the IUSTI case grouped by structured and unstructured methods. A similar spread in error levels is seen for both methods indicating that there is no discernible difference between the grid types.

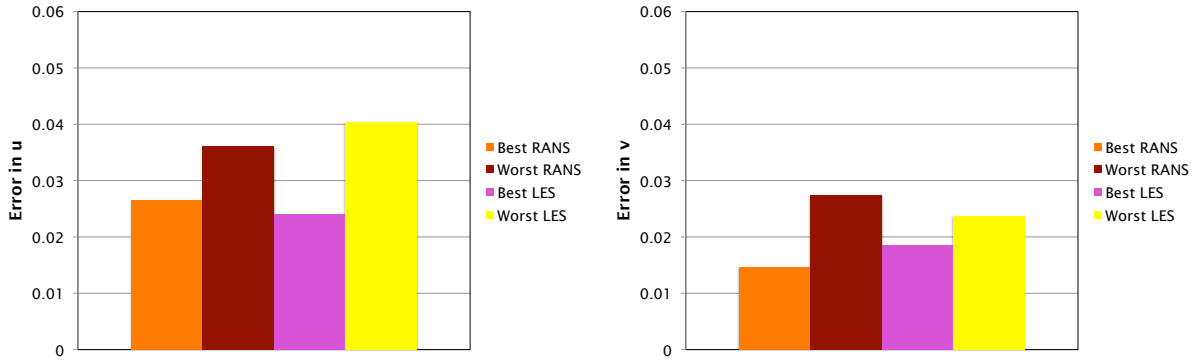

(a) error in streamwise velocity, $E(u)/U_\infty$ (b) error in transverse velocity, $E(v)/U_\infty$

Figure 27. RANS/LES comparison for the UMich. Mach 2.75, $\theta = 7.75^\circ$ case

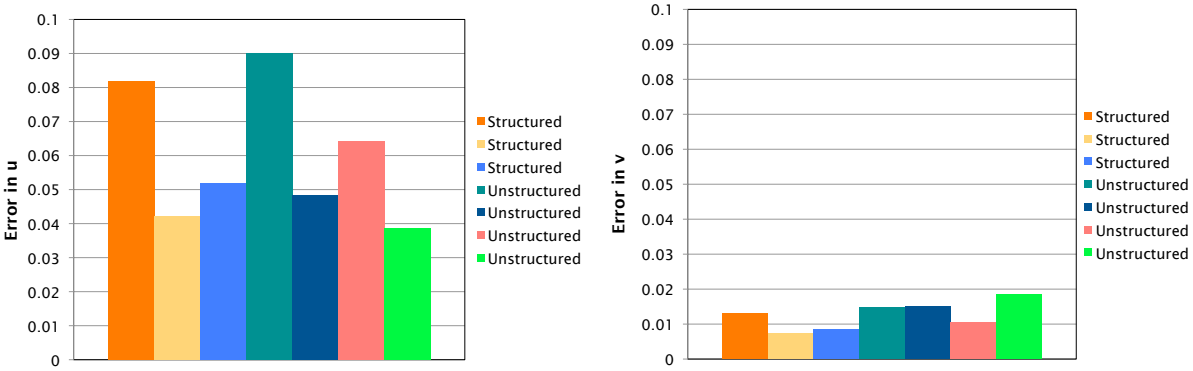

(a) error in streamwise velocity, $E(u)/U_\infty$ (b) error in transverse velocity, $E(v)/U_\infty$

Figure 28. Structured/unstructured grid comparison for the IUSTI Mach 2.25, $\theta = 8.0^\circ$ case

V. Summary and Conclusions

A workshop on the computational fluid dynamics (CFD) prediction of shock boundary-layer interactions (SBLIs) was held at the 48th AIAA Aerospace Sciences Meeting in Orlando, Florida. The purpose of the workshop was to share prediction methodologies, assess the state of the art in SBLI prediction and determine the most promising methods. Prior to the meeting four test cases were identified and contributions of solutions were solicited from the aerospace community. A total of 36 solutions from 11 contributors and 9 organizations were submitted. As part of this effort, an assessment of the submitted solutions was performed. This consisted of an assessment of the experimental data, the development of an error metric and the assessment of the CFD data using the error metric.

The experimental data for the four test cases came from two different sources: the Institut Universitaire des Systèmes Thermiques Industriels (IUSTI) in Marseilles, France and the University of Michigan (UMich.). The data used for comparison consisted of velocities and turbulent stresses measured on a plane parallel with the freestream flow and the tunnel sidewall. An uncertainty analysis of the experimental data had been previously conducted by each of the research groups involved. As part of this work a statistical uncertainty analysis of the UMich. data was performed. The analysis compared data from the streamwise and spanwise measurement planes at the locations where the planes intersected. Bi-linear interpolation was used to put the data at common points in space. The residuals for all the measured quantities were computed and the mean values of those residuals is used for the uncertainty estimate. This analysis showed the largest uncertainty was for the streamwise velocity and was (in the mean) 3.5 percent of the freestream velocity. The uncertainties in the turbulent normal stresses were found to increase linearly with the magnitude of the stress.

An error metric that represents the average error in the predicted quantity for the entire data plane was defined. This error metric was used to assess the relative quality of each of the submitted CFD solutions. Several variables were examined; streamwise velocity, u, transverse velocity, v, and turbulent stresses, $< u'^2 >$, $< v'^2 >$ and $< u'v' >$. It was found that the relative accuracy of the methods was not consistent between the variables of interest (ie. a good prediction of u did not imply a good prediction of v or any other variable for a given method). Thus, the streamwise velocity was chosen to assess the computational methods. For the most part, the submitted solutions were remarkably similar in the error levels. The primary differences between solutions were the details of the boundary-layer separation. Because of the many different methods used, the lack of consistency for the predictions and the similarity of the solutions, it was difficult to identify clear trends or single out any method as superior. In general the errors for all the solutions increased with increasing shock strength (increased deflection angle). The choice of turbulence model appears to be the dominant factor in the accuracy of the Reynolds Averaged Navier-Stokes (RANS) solutions. Large-eddy simulations had similar error levels as the RANS methods, but provided superior predictions of the normal stresses. There appeared to be no dependence on computational grid type (structured or unstructured).

The data shows that there is a need for additional research in the prediction of SBLIs. First, high quality experimental data that includes the effects of the sidewall and corner flow interactions is needed and the uncertainty of the data should be quantified. RANS turbulence models that provide normals stresses such as full Reynolds stress and algebraic Reynolds stress models should be investigated for this problem. Finally, LES methods should continue to be advanced as they show promise for this type of flow.

References

[1]Delery, J. and Marvin, J. G., "Shock-Wave Boundary Layer Interactions," AGARDograph No. 280, 1986, E. Reshotko (ed.).

[2]Benek, J., "Overview of the 2010 AIAA Shock Boundary Layer Interaction Workshop," AIAA Paper 2010-4821, 2010.

[3]Hirsch, C., "SBLI Lessons Learned - CFD Simulations of Two Test Cases ," AIAA Paper 2010-4824, 2010.

[4]Benek, J. and Babinsky, H., "Lessons Learned from the 2010 AIAA Shock Boundary Layer Interaction Workshop," AIAA Paper 2010-4825, 2010.

[5]Dupont, P., Piponniau, S., Sidorenko, A., and Debieve, J., "Investigation by Particle Image Velocimetry Measurements of Oblique Shock Reflection with Separation," *AIAA Journal*, Vol. 46, No. 6, 2008, pp. 1365–1370.

[6]*Unsteady Effects in Shock Wave Induced Separation*, edited by P. Doerffer, C. Hirsch, J.-P. Dussauge, H. Babinsky, and G. Barakos, Springer, 2010.

[7]Lapsa, A. P. and Dahm, W. J. A., "Stereo Particle Image Velocimetry of Nonequilibrium Turbulence Relaxation in a Supersonic Boundary Layer," *Experiments in Fluids*, 2010, online June 4, 2010.

[8]Dussauge, J. P., Debieve, J. F., Dupont, P., Piponniau, S., and Souverein, L. J., "Final Report on the Measurements of Shock Reflection at M=2.25," UFAST, IUSTI Deliverable No. 3.3.5, 2009.

[9]Oberkampf, W. L. and Aeschliman, D. P., "Joint Computational/Experimental Aerodynamics Research on a Hypersonic Vehicle: Part 1, Experimental Results," *AIAA Journal*, Vol. 30, No. 8, 1992.

[10]Oberkampf, W. L., Aeschliman, D. P., Henfling, J. F., and Larson, D. E., "Surface Pressure Measurements for CFD Code Validation in Hypersonic Flow." AIAA Paper 95-2273, 1995.

[11]Oberkampf, W. L. and Roy, C. J., *Verification and Validation in Scientific Computing*, Cambridge University Press, 2010.

[12]Montgomery, D. C., *Design and Analysis of Experiments*, John Wiley, 5th ed., 2000.

[13]Montgomery, D. C., *Statistics for Experimenters: Design, Innovation, and Discovery*, John Wiley, 2nd ed., 2005.

[14]Coleman, H. W. and Jr., W. G. S., *Experimentation and Uncertainty Analysis for Engineers*, John Wiley, 2nd ed., 1999.

[15]Park, M. A. and Carlson, J.-R., "Turbulent Output-Based Anisotropic Adaptation," AIAA Paper 2010-168, 2010.

[16]Pirozzoli, S. and Grasso, F., "Direct numerical simulation of impinging shock wave/turbulent boundary layer interaction at M = 2.25," *Physics of Fluids*, Vol. 18, No. 065113, 2006.

[17]Georgiadis, N. J., Rumsey, C. L., Yoder, D. A., and Zaman, K. B. M. Q., "Turbulence Modeling Effects on Calculation of Lobed Nozzle Flowfields," *Journal of Propulsion and Power*, Vol. 22, No. 3, 2006, pp. 567–575.

REPORT DOCUMENTATION PAGE		Form Approved OMB No. 0704-0188

1. REPORT DATE *(DD-MM-YYYY)*	2. REPORT TYPE	3. DATES COVERED *(From - To)*
01-03-2011	Technical Memorandum	

4. TITLE AND SUBTITLE
Assessment of Computational Fluid Dynamics (CFD) Models for Shock Boundary-Layer Interaction

5a. CONTRACT NUMBER

5b. GRANT NUMBER

5c. PROGRAM ELEMENT NUMBER

6. AUTHOR(S)
DeBonis, James, R.; Oberkampf, William, L.; Wolf, Richard, T.; Orkwis, Paul, D.; Turner, Mark, G.; Babinsky, Holger

5d. PROJECT NUMBER

5e. TASK NUMBER

5f. WORK UNIT NUMBER
WBS 984754.02.07.03.13.02

7. PERFORMING ORGANIZATION NAME(S) AND ADDRESS(ES)
National Aeronautics and Space Administration
John H. Glenn Research Center at Lewis Field
Cleveland, Ohio 44135-3191

8. PERFORMING ORGANIZATION REPORT NUMBER
E-17462

9. SPONSORING/MONITORING AGENCY NAME(S) AND ADDRESS(ES)
National Aeronautics and Space Administration
Washington, DC 20546-0001

10. SPONSORING/MONITOR'S ACRONYM(S)
NASA

11. SPONSORING/MONITORING REPORT NUMBER
NASA/TM-2011-216832

12. DISTRIBUTION/AVAILABILITY STATEMENT
Unclassified-Unlimited
Subject Categories: 02 and 07
Available electronically at http://www.sti.nasa.gov
This publication is available from the NASA Center for AeroSpace Information, 443-757-5802

13. SUPPLEMENTARY NOTES

14. ABSTRACT
A workshop on the computational fluid dynamics (CFD) prediction of shock boundary-layer interactions (SBLIs) was held at the 48th AIAA Aerospace Sciences Meeting. As part of the workshop numerous CFD analysts submitted solutions to four experimentally measured SBLIs. This paper describes the assessment of the CFD predictions. The assessment includes an uncertainty analysis of the experimental data, the definition of an error metric and the application of that metric to the CFD solutions. The CFD solutions provided very similar levels of error and in general it was difficult to discern clear trends in the data. For the Reynolds Averaged Navier-Stokes methods the choice of turbulence model appeared to be the largest factor in solution accuracy. Large-eddy simulation methods produced error levels similar to RANS methods but provided superior predictions of normal stresses.

15. SUBJECT TERMS
Shock waves; Turbulent boundary layer; Computational fluid dynamics

16. SECURITY CLASSIFICATION OF:			17. LIMITATION OF ABSTRACT	18. NUMBER OF PAGES	19a. NAME OF RESPONSIBLE PERSON
a. REPORT	b. ABSTRACT	c. THIS PAGE			STI Help Desk (email:help@sti.nasa.gov)
U	U	U	UU	34	19b. TELEPHONE NUMBER *(include area code)* 443-757-5802